Viel et al. reported the conjugation of ^{18}F to oligonucleotide by using (*N*-[3-(2-[^{18}F]fluoropyridin-3-yloxy)-propyl]-2-bromoacetamide ([^{18}F]FRyBrA), and this method also required the annealing process (*10, 11*). In spite of their efforts, detail pharmacokinetic information about naked siRNA or siRNA in DDS carriers is still largely lacking.

In the present study, we developed a novel technique for labeling siRNA with a positron emitter, ^{18}F, in which double-stranded siRNA was labeled to gain conformational accuracy for examining the pharmacokinetics of siRNA by using [^{18}F]SFB as an ^{18}F labeling reagent. [^{18}F]SFB have been widely used to form a stable amide bond by reacting with primary amino groups for a short time and very easily for labeling certain peptides (*12*), antibodies (*13*), or DNA oligonucleotides (*14*). Because ^{18}F has an extremely short half-life (109 min), avoidance of the annealing process by labeling of double-stranded siRNA is favorable. [^{18}F]-labeled siRNA thus prepared was identified by ESI-TOF-MS, HPLC, and autoradiography after electrophoresis. By use of this positron emitter-labeled siRNA, we actually examined the biodistribution of siRNA by PPIS in the presence or absence of cationic liposome, a DDS carrier of siRNA. We also performed NIRF imaging for verifying the in vivo behavior of siRNA and discussed the correspondence of the imaging results obtained from NIRF imaging and PPIS imaging.

EXPERIMENTAL PROCEDURES

Materials. 4,7,13,16,21,24-Hexaoxa-1,10-diazabicyclo[8.8.8]-hexacosane (K[2.2.2]), tetra-*n*-propyl-ammonium hydroxide (Pr_4NOH), *N,N,N′,N′*-tetramethyl-*O*-(*N*-succinimidyl)uronium tetrafluoroborate (TSTU), CH_3CN (anhydrous), and fetal bovine serum were obtained from Sigma-Aldrich (Saint Louis, MO, USA). Potassium carbonate·1.5H_2O was purchased from Merck (Darmstadt, Germany). Anion-exchange resin AG1-X8 (OH^- form, 100−200 mesh) was from Bio-Rad Laboratories (Hercules, USA). *N,N*-Dimethylformamide (DMF) was purchased from Wako Pure Chemical Industries, Ltd. (Osaka, Japan). A cationic lipid for transgene use, 1,2-dioleoyl-3-trimethylammonium-propane (DOTAP), was purchased from Avanti Polar Lipids Inc. (Alabaster, AL, USA). Cholesterol was kindly provided by Nippon Fine Chemical Co., Ltd. (Takasago, Hyogo, Japan). Trizol reagent was obtained from Invitrogen Co. (Carlsbad, CA). An alfalfa-free feed was purchased from Oriental Yeast co. Ltd. (Tokyo, Japan). Escain was purchased from Mylan Pharmaceuticals (Morgantown, WV). All other chemicals and solvents were analytical grade and were used without further purification unless otherwise stated. [^{18}F]Fluoride was produced with a cyclotron (HM-18, Sumitomo Heavy Industries, Tokyo, Japan) at Hamamatsu Photonics PET Center by the ^{18}O(p,n)^{18}F nuclear reaction using [^{18}O]H_2O. Labeled compounds were synthesized by using modified CUPID system (Sumitomo Heavy Industries, Tokyo, Japan). The HPLC column used for the purification of succinimidyl 4-[^{18}F] fluorobenzoate ([^{18}F]SFB) was an Inertsil ODS3 (10 × 250 mm, 5 μm, GL Sciences Inc., Tokyo, JAPAN). Nonradioactive fluorine-conjugated siRNA was identified by using a UPLC/ESI-QTOF-MS system, which consisted of an ACQUITY ultraperformance liquid chromatography (UPLC) system and an electrospray ionization quadrupole time-of-flight mass spectrometer (SYNAPT High Definition Mass Spectrometry system; Waters, Milford, MA, USA). An ultraviolet−visible (UV/vis) detector (ACQUITY TUV, Waters) was used. The UPLC column used for the identification of fluorine-labeled siRNA was an Acquity UPLC BEH C18 column (2.1 × 100 mm, 1.7 μm, Waters Corp.). The particle size and zeta-potential of nanoparticles were measured by using a Zetasizer Nano ZS (Malvern, Worcs, UK). Gel for obtaining an autoradiogram of ^{18}F and siRNA after electrophoresis was used an FLA-7000 (FUJIFILM Corporation, Tokyo, Japan) and LAS-3000 mini system (Fuji Film, Tokyo, Japan), respectively. Fluorescence imaging was performed by using a Xenogen IVIS Lumina System coupled to *Living Image* software for data acquisition (Xenogen Corp., Alameda, CA). PET imaging was performed by using a planar positron imaging system (PPIS, Hamamatsu Photonics, Shizuoka, Japan). Radioactivities in each organs were measured by gamma-counter (ARC-2000, Aloka, Tokyo, Japan).

Experimental Animals. Five-week-old male BALB/c mice male were purchased from Japan SLC Inc. (Shizuoka, Japan). The animals were cared for according to the Animal Facility Guidelines of the University of Shizuoka. All animal experiments were approved by the Animal and Ethics Review Committee of the University of Shizuoka.

siRNA Sequence. Alexa Fluor 750-labeled siRNA (AF750-siRNA) was purchased from Japan Bio Services Co., Ltd. (Saitama, Japan). Antisense strand contained a fluorescence at the 3′ end of the strand. siRNA for positron emitter-labeling was synthesized and purified by Hokkaido System Science. The nucleotide sequences of the siRNA were those of an unspecific scrambled RNA, and the antisense strand contained a 3′ amino C6 linker for the radioactive labeling of the siRNA duplex (Scheme 1). The sequences of the siRNA used were 5′-CGAUUCGCUAGACCGGCUUCAUUGCAG-3′ (sense) and 5′-GCAAUGAAGCCGGUCUAGCGAAUCGAU-3′ (antisense).

Synthesis of Ethyl-(4-Trimethylammonium)benzoate Trifluoromethanesulfonate. Ethyl 4-dimethylaminobenzoate was synthesized according to the procedure reported by Haka et al. (*15*). The synthetic compound was assigned by ^{1}H NMR and ^{13}C NMR. Ethyl 4-dimethylaminobenzoate 11.4 g (59 mmol) was dissolved in 70 mL anhydrous CH_2Cl_2. Ten grams of $CF_3SO_3CH_3$ (64.9 mmol) was added dropwise to the solution, and the mixture was stirred overnight at room temperature. A crystalline precipitate was formed by the addition of Et_2O (100 mL) and collected by suction filtration. Recrystallization from CH_2Cl_2/Et_2O gave 10.2 g (48%) of ethyl 4-trimethylammoniumbenzoate trifluoromethanesulfonate.

Radiosynthesis of [^{18}F]KF/K[2,2,2] Complex. [^{18}F]KF/K-[2,2,2] was obtained by use of a previously reported method (*16*). In brief, [^{18}F]fluoride was trapped by ion-exchange resin AG1-X8 and eluted from the resin by 0.5 mL of 40 mM K_2CO_3. To this fluoride solution, 15 mg of K[2,2,2] in CH_3CN (2 mL) was added. Water was removed by azeotropic distillation at 110 °C under He flow (400 mL/min) for 5 min. To the residue, the addition of CH_3CN (1 mL) and azeotropic distillation were repeated twice. Then, the residue was dried under reduced pressure for 1 min, and the reaction vessel was purged with a flow of He (50 mL/min) for 1 min to ensure complete dryness. Finally, the reaction vessel was cooled to room temperature and used for further labeling.

Preparation of Succinimidyl 4-[^{18}F]fluorobenzoate ([^{18}F]-SFB). [^{18}F]SFB was prepared according to the one-pot procedure of Tang et al. (*17*) with some modifications. The precursor (5 mg) in 1.5 mL of CH_3CN was added to the dried [^{18}F]KF/K[2,2,2] complex mentioned above and reacted at 80 °C for 10 min. After the reaction mixture had been cooled, 20 μL of 1 M Pr_4NOH in 0.5 mL of CH_3CN was added; and hydrolysis was carried out at 120 °C for 5 min. Then, to the reaction mixture, TSTU (15 mg) in 0.5 mL of CH_3CN was added and converted to [^{18}F]SFB at 80 °C for 5 min. The reaction mixture was diluted with 2.0 mL of 5% CH_3COOH and transferred to the HPLC injector. Crude product was purified by semipreparative HPLC (CH_3CN:H_2O = 300:700, 6 mL/min, 254 nm). The radioactive peak eluted at 25.7 min was collected, diluted with 30 mL of H_2O, and passed through a Sep-Pak C18 cartridge (Waters). [^{18}F]SFB retained on the cartridge was released with 4 mL of CH_2Cl_2 and recovered into a V-vial by passage through a Sep-Pak Dry cartridge (Waters). Then, the [^{18}F]SFB was concen-

Scheme 1. Synthesis of the [^{18}F]SFB and [^{18}F]-Labeled siRNA

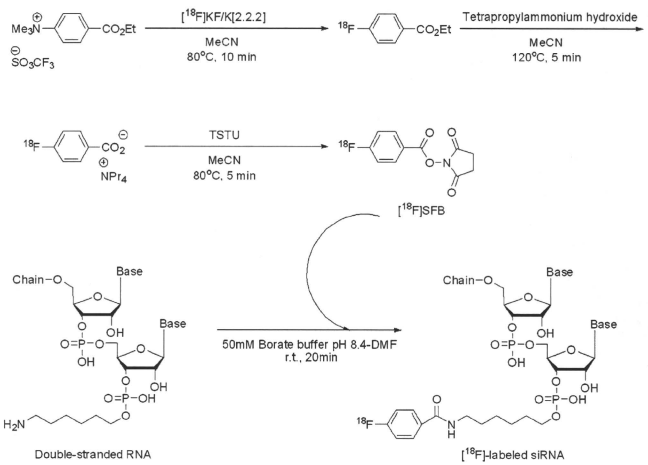

Table 1. Gradient Flow Table

time (min)	0.1 M TEAA (%)	CH_3CN (%)	flow rate (mL/min)
0–2	95–90	5–10	0.3
2–3	90–75	10–25	0.3
3–7	75–60	25–40	0.3
7–10	60–0	40–100	0.3

trated by a flow of He (200 mL/min) at 60 °C and used for labeling. [^{18}F]SFB with (a specific radioactivity of 51.4 GBq/μmol, a radiochemical yield of 21.1%) was obtained.

Radiolabeling of siRNA with [^{18}F]SFB. siRNA (40 nmol) in 16 μL of 50 mM borate buffer, pH 8.5, was added to the [^{18}F]SFB (60 nmol) in 3.6 μL of DMF. The mixture was vortexed for a few seconds and then incubated at room temperature for 20 min. The reaction mixture was purified and concentrated by ultrafiltration through a 10 000 molecular weight cutoff filter (Amicon, Millipore, Bedford, MA, USA). The mixture was centrifuged at 4000 × *g* with RNase-free phosphate-buffered saline (PBS). [^{18}F]-labeled siRNA with a radiochemical yield of 37.9% and a specific activity of 25.5 GBq/μmol was obtained. Nonradioactive fluorine-conjugated siRNA was synthesized in a similar manner except that 150 nmol cold SFB was used instead of 60 nmol [^{18}F]SFB.

Analytical Methods. Nonradioactive fluorine-conjugated siRNA was identified by using a UPLC/ESI-QTOF-MS system. The analytical column was maintained at 40 °C. A ultraviolet–visible (UV/vis) detector, equipped with a 500 nL flow cell, was also directly connected between the column outlet and the QTOF-MS instrument. Fractionation of fluorine-conjugated siRNA was performed at a flow rate of 0.3 mL/min using as the eluent the gradient of 0.1 M triethylammonium acetate (TEAA, pH 7.0) and CH_3CN. Gradient profile is presented in the Table 1.

Evaluation of siRNA Labeling. Precursor siRNA, fluorine-conjugated siRNA (non-RI), and [^{18}F]-labeled siRNA (0.5 μg) were applied to a 15% polyacrylamide gel and electrophoresed. Then, the gel was exposed to an imaging plate for obtaining an autoradiogram of ^{18}F by using an FLA-7000; the gel was stained for 5 min in ethidium bromide (EtBr), and siRNA was detected by using a LAS-3000 mini system.

Preparation of Cationic Liposomes and Their Complexes with siRNA. DOTAP and cholesterol (1:1 as a molar ratio) were dissolved in *tert*-butyl alcohol for freeze–drying and hydrated in RNase-free PBS. The liposomes were frozen and thawed for 3 cycles using liquid nitrogen and extruded 10 times through a polycarbonate membrane filter having a pore size of 100 nm (Nucleopore, Maidstone, UK). Then, the cationic liposome and siRNA were mixed gently and incubated for 10 min at room temperature to form liposome/siRNA complexes. The nitrogen moiety of cationic liposome to the phosphorus of siRNA (N/P ratio) was 24:1 in the complexes. The particle size and zeta-potential of liposome/siRNA complexes diluted with RNase-free PBS were measured. The particle size of liposome/siRNA complexes was 218 ± 3.0 nm (n = 3), and the particles showed monodispersion (polydispersity index = 0.16). The zeta-potential was 36.3 ± 1.9 mV.

Near-Infrared Fluorescence Imaging in Vivo. The biodistribution of AF750-siRNA was assessed by using an IVIS Lumina System. Mice were fed an alfalfa-free feed to reduce the effect of background fluorescence. The animals were anesthetized continuously via inhalation of 2% escain. siRNA or liposome/siRNA complexes containing 15 μg AF750-siRNA were injected via a tail vein under anesthesia. Alexa Fluor 750 fluorescence was acquired every 10 min for up to 60 min after the injection. After monitoring, the mice were sacrificed under anesthesia. Then, the organs, namely, heart, lungs, liver, spleen, and kidneys, were collected and imaged ex vivo with the IVIS.

PPIS Imaging of [^{18}F]-Labeled siRNA. Biodistribution of [^{18}F]-labeled siRNA was imaged noninvasively by using a PPIS (*18–20*). Animals were anesthetized with an intraperitoneal injection of pentobarbital at 50 mg/kg, and then fixed on an animal holder. To determine the whole-body biodistribution of siRNA, we administered the [^{18}F]-labeled siRNA intravenously (2.5 MBq/mouse). The scan was started immediately after the administration and performed for 60 min. Images were analyzed by using software *ImageJ*. After the PPIS scan, the mice were sacrificed for the collection of the blood from a carotid artery under anesthesia. Then, the heart, lungs, liver, spleen, and kidneys were removed, and the biodistribution of

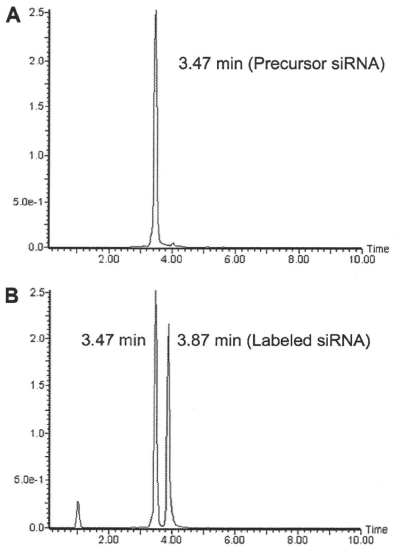

Figure 1. UPLC analysis of fluorine-conjugated siRNA. Nonradioactive fluorine was conjugated to siRNA and separated with the UPLC system. (A) Peak of precursor siRNA at 3.47 min. (B) Peaks of unreacted siRNA at 3.47 min and fluorine-labeled siRNA at 3.87 min after the reaction.

[^{18}F]-labeled siRNA was measured with a gamma counter. Distribution data were presented as percent dose per wet tissue. The total volume of blood was assumed to be 7.56% of the body weight. A time−activity curve was obtained from the mean pixel radioactivity in the region of interest (ROI) of the PPIS images.

Evaluation of siRNA Stability against Serum-Mediated Degradation. Fluorine-conjugated (0.5 μg) naked siRNA or that complexed with liposomes was incubated in 90% fetal bovine serum for 60 min at 37 °C. The siRNA was extracted from the serum by using Trizol reagent and subjected to 15% polyacrylamide gel electrophoresis. The gel was stained for 5 min in EtBr, and siRNA was detected by using a LAS-3000 mini system.

RESULTS

[^{18}F]-Labeling of siRNA and Its Radiochemistry. The methods for synthesis of [^{18}F]SFB and [^{18}F]-labeling of siRNA are shown in Scheme 1. At first, we prepared non-radioisotope (non-RI) fluorine-conjugated siRNA and identified the compound by using LC/ESI-TOF-MS (Table 1). Unreacted siRNA showed a peak at 3.47 min (Figure 1A). After the reaction, HPLC analysis indicated 2 main peaks, namely, labeled siRNA at 3.87 min and precursor siRNA at 3.47 min, respectively (Figure 1B). These peaks were fractionated by HPLC and analyzed by ESI-TOF-MS, giving multiply charged ion peaks of *m/z* $[M\text{-}8H]^{8-}$ 2196.1, $[M\text{-}7H]^{7-}$ 2510.9, and $[M\text{-}6H]^{6-}$ 2930.0 (data not shown), which corresponded to the labeled siRNA (expected mass of *m/z* $[M\text{-}8H]^{8-}$ 2196.7, $[M\text{-}7H]^{7-}$ 2510.7, and $[M\text{-}6H]^{6-}$ 2929.3). The overall yield of labeled siRNA was greater than 30% based on the peak area. On the basis of the result from non-RI fluorine-grafting to siRNA, [^{18}F]-labeled siRNA was prepared according to the same procedure, and then electrophoresis assay and subsequent autoradiography were performed to confirm the production of [^{18}F]-labeled siRNA. Electrophoresis assay with an imaging plate showed that the siRNA was labeled with [^{18}F]-fluorine without any other exposure bands (Figure 2). In addition, the main band visualized by EtBr staining showed the same position as the band on the same polyacrylamide gel observed by autoradiography. As a result, [^{18}F]-labeled siRNA was successfully prepared without any positron emitter-labeled byproducts, and the labeled siRNA was not degraded under the experimental conditions used.

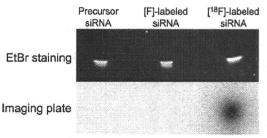

Figure 2. Demonstration of [^{18}F] labeling of siRNA. Precursor siRNA, fluorine-conjugated siRNA, and [^{18}F]-labeled siRNA were applied to a 15% polyacrylamide gel, electrophoresed, and stained with ethidium bromide. The gel was exposed to an imaging plate for detecting ^{18}F.

Biodistribution of siRNA Determined with near-Infrared Fluorescence Imaging in Vivo. We examined the in vivo behavior of siRNA by use of the NIRF imaging system. Mice were intravenously administered naked AF750-siRNA or liposome/AF750-siRNA complexes via a tail vein. The fluorescence imaging of AF750-siRNA was started immediately after the injection and monitored for 60 min. The biodistribution of AF750-siRNA is shown in Figure 3. The results indicated that the fluorescence compound was accumulated in the bladder immediately after the administration of naked AF750-siRNA and then excreted in the urine (Figure 3A). On the contrary, fluorescence was observed at the upper part of the body where the lung was positioned after the administration of liposome/AF750-siRNA complexes. The total fluorescence intensity of the image of mice injected with naked AF750-siRNA was apparently higher than that obtained with the liposomal formulation: Fluorescence in bladder after injection of naked siRNA was quite intense because bladder is located near the body surface, while that in lungs after injection of cationic liposome complexes was weak because lungs are located more deep from body surface compared with bladder.

The ex vivo imaging showed that a small amount of fluorescence remained in the kidneys but that no fluorescence was detected in the other tissues examined (Figure 3B). In contrast, the fluorescence of the cationic liposome/AF750-siRNA complexes accumulated in the lungs, being consistent with the in vivo imaging data.

Stability of Fluorine-Conjugated siRNA against Serum-Mediated Degradation. We evaluated the stability of naked fluorine-conjugated siRNA and cationic liposome/fluorine-conjugated siRNA complexes in serum for 60 min (Figure 4). The naked fluorine-conjugated siRNA incubated in PBS (control) was not decomposed. However, the band of naked siRNA obtained by electrophoresis of the sample that had been incubated in the presence of serum disappeared, indicating that the siRNA had been degraded by RNase within 60 min. In contrast, the band of siRNA was detected in the case of the cationic liposome/siRNA complexes exposed to the serum, indicating that complex formation protected siRNA from RNase in the serum.

In Vivo PPIS Imaging of siRNA Trafficking. Next, we examined [^{18}F]-labeled siRNA trafficking by use of PPIS. Mice were intravenously administered naked [^{18}F]-labeled siRNA in

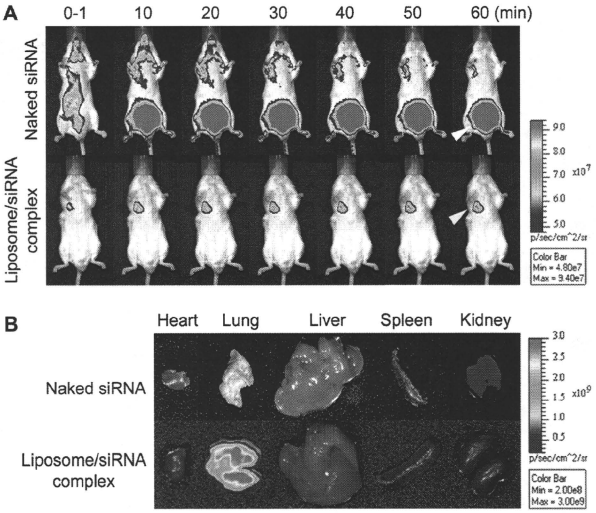

Figure 3. NIRF in vivo imaging with AF750-siRNA and liposome/AF750-siRNA complexes. (A) AF750- siRNA (top) or liposome/AF750-siRNA complexes (bottom) were intravenously administered to BALB/c mice. Images were acquired every 10 min for up to 60 min after the administration. The white arrowhead shows the bladder region, and the yellow arrowhead, the lung region. (B) Ex vivo imaging of AF750-siRNA and liposome/AF750-siRNA complexes at 60 min after administration.

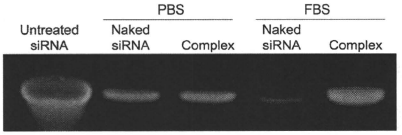

Figure 4. Stability of naked siRNA or liposome/siRNA complexes in FBS. siRNA (0.5 μg) was incubated with PBS (−) or 90% FBS at 37 °C for 60 min. siRNA was extracted and electrophoresed on a 15% polyacrylamide gel after a 60 min incubation and stained with EtBr. Untreated siRNA was used as a control marker.

PBS (−) or liposome/[^{18}F]-labeled siRNA complexes via a tail vein. The real-time imaging of [^{18}F]-labeled siRNA using PPIS was acquired for 60 min, and images were integrated every 5 min (Figure 5A). The ^{18}F radioactivity of the naked [^{18}F]-labeled siRNA accumulated inside the kidneys immediately after administration. This accumulation was not detected in NIRF in vivo imaging because of the influence of tissue depth. Then, ^{18}F was transferred to the bladder and subsequently excreted in the urine. In contrast, most of the ^{18}F radioactivity after the administration of cationic liposome/[^{18}F]-labeled siRNA complexes were retained in the lungs for 60 min, and only insignificant accumulation of them was observed in the bladder. The time−activity curve of ^{18}F in naked siRNA showed transient accumulation in kidney immediately after injection (19% injected dose/tissue at 2 min), and half of that was transferred to bladder at 21 min, and then the excretion of ^{18}F to bladder was gradually increased (Figure 5B). In contrast, the most of the ^{18}F after injection of liposome/siRNA complexes immediately accumulated in lungs and was maintained up to 60 min (76% injected dose/tissue). The biodistribution data obtained with a gamma counter after organ dissection showed that the ^{18}F after administration of naked [^{18}F]-labeled siRNA had not been distributed in any tissues tested, whereas the radioactivity after the injection of the cationic liposome/[^{18}F]-labeled siRNA complexes was highly distributed in the lungs (Figure 5C). These results corresponded roughly to the data obtained from the fluorescence ex vivo imaging.

Moreover, to confirm whether the accumulation of ^{18}F in the lungs after administration of cationic liposome/[^{18}F]-labeled siRNA reflected the accumulation of the liposomes of the complex, we examined the biodistribution of cationic liposome/siRNA complexes prepared with [^{3}H]cholesterylhexadecyl ether as a component. As a result, the liposomal complexes with siRNA were distributed in the lungs quite similarly to the distribution of the ^{18}F, suggesting that cationic liposome/siRNA accumulated in lungs as the complex form (Supporting Information Figure S1).

DISCUSSION

Recently, the topical application of siRNA medicines has reached clinical trial, and siRNA delivery systems for systemic injection have been extensively studied for the next generation of siRNA medicines (*21*). Pharmacokinetic information on siRNA molecules is considered to be particularly important for the acceleration of the development of siRNA medicine. Among the technologies for pharmacokinetic analysis, PET imaging technique is considered to be applicable to both preclinical trial and microdosing study (human phase 0 study). Using subtoxic and subpharmacologic doses, PET microdosing studies can be performed to screen for drug candidates for clinical trials on the basis of their pharmacokinetic properties (*22, 23*).

In the present study, we labeled double-stranded siRNA with^{18}F to obtain pharmacokinetics information about siRNA and siRNA in DDS carriers. We used [^{18}F]-fluorine as a short-

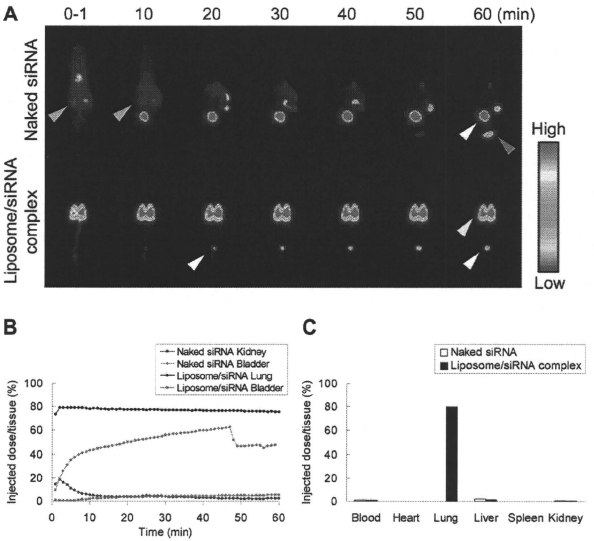

Figure 5. PPIS imaging with [^{18}F]-labeled siRNA and liposome/[^{18}F]-labeled siRNA complexes. (A) Naked siRNA (top) or liposome/siRNA complexes (bottom) at 2.5 MBq in 0.2 mL were intravenously administered to BALB/c mice. Images were acquired with a 1 min frame at 1, 10, 20, 30, 40, 50, and 60 min after the administration. The green arrowhead shows kidneys; the white one, the bladder; the red one, urine; and the yellow one, the lungs. (B) Real-time changes in [^{18}F]-labeled siRNA and liposomal [^{18}F]-labeled siRNA. Time activity curves of ^{18}F with naked siRNA shows kidney (blue) and bladder (red) and that of ^{18}F with cationic liposome/siRNA shows lung (black) and bladder (green). (C) After the PPIS scan, the mice were sacrificed, and biodistribution of ^{18}F in each organ was then measured with a gamma counter.

lived positron-emitting radionuclide (half-life: 109 min), which has been applied to humans for cancer diagnosis in the form of [2-^{18}F]2-deoxy-2-fluoroglucose ([^{18}F]FDG). The advantages of the present methodology to label siRNA are that (1) the modification of double-stranded RNA with amino group enables fast preparation and purification without the time-consuming process of annealing and (2) the methodology maintains the conformational accuracy of the siRNA. Indeed, reaction of siRNA and [^{18}F]SFB was complete within 20 min. In addition, fluorine-conjugated siRNA was identified by LC and ESI-TOF-MS (Figure 1) and did not decompose during the reaction or purification process (Figure 2).

It is well-known that one of the most important factors regarding the biodistribution of liposomes in vivo is the charge of the liposomal surface. Positively charged complexes aggregate in the presence of serum proteins (*24*), are entrapped in the lung capillaries, and thus accumulate in the lung tissue (*25, 26*) after intravenous administration. In fact, when liposomes were labeled with [^{3}H]cholesterylhexadecyl ether, the radioactivity of cationic liposome/siRNA complexes accumulated in the lungs (Supporting Information Figure S1). However, since nucleic acids such as siRNAs and oligodeoxynucleotides (ODNs) are known to be eliminated from the circulation via the kidneys and excreted into the urine 60 min after administration via a tail vein (*27, 28*), distribution studies on siRNAs or ODNs besides on their carriers are important for the development of nucleic acid medicines. In the distribution study, [^{3}H]cholesterylhexadecyl ether was accumulated in the liver to some extent, although the accumulation of siRNA was not observed after injection of cationic liposome/siRNA complex. We speculate that siRNA was degraded in the liver and excreted, while cholesterylhexadecyl ether did not.

In the present study, we first used AF750-siRNA and examined its in vivo behavior by using NIRF fluorescence imaging. NIRF fluorescence was rapidly cleared from the bloodstream and excreted in the bladder after the administration of naked AF750-siRNA (Figure 3). In contrast, the fluorescence of cationic liposome/siRNA complexes accumulated in the lungs. However, the differential fluorescence intensities between in vivo images and ex vivo ones indicated the limitation of NIRF imaging. Quantitative analysis could not be applied due to the influence of tissue depth on the fluorescence intensity. Moreover, it is possible that fluorescence self-quenching and/or resonance energy transfer affect the intensity.

In contrast to NIRF imaging, PPIS or PET technology provides quantitative analytic data with high spatial resolution. ^{18}F was observed in the kidneys until 10 min after the administration of naked [^{18}F]-labeled siRNA, and subsequently, it was transferred to the bladder and excreted into urine (Figure 5). This result is consistent with previous result reported by Viel et al. who used ^{18}F-labeled naked siRNA (*11*). Other reports also presented the renal excretion of siRNA (*27, 29, 30*). In addition, Bartlett et al. reported that the excretion of ^{64}Cu-labeled naked siRNA was quite fast (*9*). They indicated that the siRNA in a complex with cyclodextrin-containing polycation excreted quite rapidly and suggested the instability of the complex. Therefore, determination of siRNA trafficking instead of carrier trafficking is important for the development of siRNA medicines. In contrast to the in vivo fate of naked siRNA, the ^{18}F of

cationic liposome/[^{18}F]-labeled siRNA complexes was spread throughout the lungs and was retained in them at least up to 60 min.

Next, we investigated the stability of siRNA in the presence of serum by performing an electrophoresis assay. The data indicated that naked siRNA was degraded when incubated for 60 min in serum, whereas the liposome/siRNA complexes were not (Figure 4). These results suggest that naked siRNA has a short half-life in vivo and is rapidly eliminated by renal excretion as a degraded form. However, further study is needed to clarify whether the excreted siRNA is in the intact form or degraded form. On the other hand, a part of the ^{18}F showed enterohepatic circulation. This enterohepatic circulation would be mediated by some of the fragmented siRNA having the polar moiety (the alkyl chain on the 3′ end of the antisense strand) and nonpolar moiety (siRNA).

As indicated above, the serum stability study showed that the liposomal siRNA was not degraded in the presence of serum. Furthermore, the ^{18}F distribution of liposomal [^{18}F]-labeled siRNA was similar to the distribution of the [^{3}H]-labeled liposome carrier: Both were accumulated in the lungs after intravenous administration. Taken together, our data strongly suggest that liposomal siRNA would be delivered to the lungs in its intact form. In conclusion, we developed a novel positron emitter-labeling methodology for siRNA and evaluated the in vivo trafficking of [^{18}F]-labeled siRNA by PPIS. The results of present study suggest that siRNA is stable as a complex with liposomes and should be deliverable specific tissues depending on the characteristics of the carrier. Therefore, designing the DDS carrier expands the usefulness of siRNA in vivo, and the present technology might support the development of siRNA medicines.

ACKNOWLEDGMENT

This study was financially supported by the Health and Labor Sciences Research Grants from the Ministry of Health, Labour, and Welfare of Japan. Synthesis of positron emitter-labeled siRNA was supported in part by Hokkaido System Science Co. Ltd. We thank Drs. T. Kakiuchi and H. Uchida at Hamamatsu Photonics K.K. PET Center for PET study for their technical assistance. They also thank Drs. S. Akai and T. Toyo'oka at the University Shizuoka for their valuable discussions as well as for allowing us to use their facilities. We also acknowledge Dr. S. Inagaki for helpful discussions and excellent technical assistance.

Supporting Information Available: Preparation of [^{3}H]-labeled liposome and complex. Biodistribution of liposomes and complexes. This material is available free of charge via the Internet at http://pubs.acs.org.

LITERATURE CITED

(1) Fire, A., Xu, S., Montgomery, M. K., Kostas, S. A., Driver, S. E., and Mello, C. C. (1998) Potent and specific genetic interference by double-stranded RNA in Caenorhabditis elegans. *Nature 391*, 806–811.

(2) Elbashir, S. M., Harborth, J., Lendeckel, W., Yalcin, A., Weber, K., and Tuschl, T. (2001) Duplexes of 21-nucleotide RNAs mediate RNA interference in cultured mammalian cells. *Nature 411*, 494–498.

(3) Pai, S. I., Lin, Y. Y., Macaes, B., Meneshian, A., Hung, C. F., and Wu, T. C. (2006) Prospects of RNA interference therapy for cancer. *Gene Ther. 13*, 464–477.

(4) Jeong, J. H., Mok, H., Oh, Y. K., and Park, T. G. (2009) siRNA conjugate delivery systems. *Bioconjugate Chem. 20*, 5–14.

(5) Zimmermann, T. S., Lee, A. C. H., Akinc, A., Bramlage, B., Bumcrot, D., Fedoruk, M. N., Harborth, J., Heyes, J. A., Jeffs, L. B., John, M., Judge, A. D., Lam, K., McClintock, K., Nechev, L. V., Palmer, L. R., Racie, T., Rohl, I., Seiffert, S., Shanmugam, S., Sood, V., Soutschek, J., Toudjarska, I., Wheat, A. J., Yaworski, E., Zedalis, W., Koteliansky, V., Manoharan, M., Vornlocher, H. P., and MacLachlan, I. (2006) RNAi-mediated gene silencing in non-human primates. *Nature 441*, 111–114.

(6) Kim, S. H., Jeong, J. H., Lee, S. H., Kim, S. W., and Park, T. G. (2008) LHRH receptor-mediated delivery of siRNA using polyelectrolyte complex micelles self-assembled from siRNA-PEG-LHRH conjugate and PEI. *Bioconjugate Chem. 19*, 2156–2162.

(7) Medarova, Z., Pham, W., Farrar, C., Petkova, V., and Moore, A. (2007) In vivo imaging of siRNA delivery and silencing in tumors. *Nat. Med. 13*, 372–377.

(8) Urakami, T., Akai, S., Katayama, Y., Harada, N., Tsukada, H., and Oku, N. (2007) Novel amphiphilic probes for [^{18}F]-radiolabeling preformed liposomes and determination of liposomal trafficking by positron emission tomography. *J. Med. Chem. 50*, 6454–6457.

(9) Bartlett, D. W., Su, H., Hildebrandt, I. J., Weber, W. A., and Davis, M. E. (2007) Impact of tumor-specific targeting on the biodistribution and efficacy of siRNA nanoparticles measured by multimodality *in vivo* imaging. *Proc. Natl. Acad. Sci. U.S.A. 104*, 15549–15554.

(10) Viel, T., Kuhnast, B., Hinnen, F., Boisgard, R., Tavitian, B., and Dolle, F. (2007) Fluorine-18 labelling of small interfering RNAs (siRNAs) for PET imaging. *J. Labelled Compd. Radiopharm. 50*, 1159–1168.

(11) Viel, T., Boisgard, R., Kuhnast, B., Jego, B., Siquier-Pernet, K., Hinnen, F., Dolle, F., and Tavitian, B. (2008) Molecular imaging study on *in vivo* distribution and pharmacokinetics of modified small interfering RNAs (siRNAs). *Oligonucleotides 18*, 201–212.

(12) Chen, X., Park, R., Shahinian, A. H., Tohme, M., Khankaldyyan, V., Bozorgzadeh, M. H., Bading, J. R., Moats, R., Laug, W. E., and Conti, P. S. (2004) 18F-labeled RGD peptide: initial evaluation for imaging brain tumor angiogenesis. *Nucl. Med. Biol. 31*, 179–189.

(13) Vaidyanathan, G., and Zalutsky, M. R. (1994) Improved synthesis of N-succinimidyl 4-[^{18}F]fluorobenzoate and its application to the labeling of a monoclonal-antibody fragment. *Bioconjugate Chem. 5*, 352–356.

(14) Li, J., Trent, J. O., Bates, P. J., and Ng, C. K. (2006) Labeling G-rich oligonucleotides (GROs) with N-succinimidyl 4-[^{18}F]fluorobenzoate (S18FB). *J. Labelled Compd. Radiopharm. 49*, 1213–1221.

(15) Haka, M. S., Kilbourn, M. R., Watkins, G. L., and Toorongian, S. A. (1989) Aryltrimethylammonium trifluoromethanesulfonates as precursors to aryl [^{18}F] fluorides: improved synthesis of [^{18}F] GBR-13119. *J. Labelled Compd. Radiopharm. 27*, 823–833.

(16) Harada, N., Ohba, H., Fukumoto, D., Kakiuchi, T., and Tsukada, H. (2004) Potential of [^{18}F]β-CFT-FE (2β-carbomethoxy-3β-(4-fluorophenyl)-8-(2-[^{18}F]fluoroethyl)nortropane) as a dopamine transporter ligand: A PET study in the conscious monkey brain. *Synapse 54*, 37–45.

(17) Tang, G., Zeng, W. B., Yu, M. X., and Kabalka, G. (2008) Facile synthesis of N-succinimidyl 4-[^{18}F]fluorobenzoate ([^{18}F]SFB) for protein labeling. *J. Labelled Compd. Radiopharm. 51*, 68–71.

(18) Takamatsu, H., Kakiuchi, T., Noda, A., Uchida, H., Nishiyama, S., Ichise, R., Iwashita, A., Mihara, K., Yamazaki, S., Matsuoka, N., Tsukada, H., and Nishimura, S. (2004) An application of a new planar positron imaging system (PPIS) in a small animal: MPTP-induced parkinsonism in mouse. *Ann. Nucl. Med. 18*, 427–431.

(19) Uchida, H., Okamoto, T., Ohmura, T., Shimizu, K., Satoh, N., Koike, T., and Yamashita, T. (2004) A compact planar positron imaging system. *Nucl. Instrum. Methods Phys. Res., Sect. A 516*, 564–574.

(20) Uchida, H., Sato, K., Kakiuchi, T., Fukumoto, D., and Tsukada, H. (2008) Feasibility study of quantitative radioactivity monitoring of tumor tissues inoculated into mice with a planar positron imaging system (PPIS). *Ann. Nucl. Med. 22*, 57–63.
(21) de Fougerolles, A. R. (2008) Delivery vehicles for small interfering RNA *in vivo*. *Hum. Gene Ther. 19*, 125–32.
(22) Bauer, M., Wagner, C. C., and Langer, O. (2008) Microdosing studies in humans: the role of positron emission tomography. *Drugs in R&D 9*, 73–81.
(23) Wagner, C. C., Muller, M., Lappin, G., and Langer, O. (2008) Positron emission tomography for use in microdosing studies. *Curr. Opin. Drug Discovery Dev. 11*, 104–110.
(24) Litzinger, D. C., Brown, J. M., Wala, I., Kaufman, S. A., Van, G. Y., Farrell, C. L., and Collins, D. (1996) Fate of cationic liposomes and their complex with oligonucleotide *in vivo*. *Biochim. Biophys. Acta, Biomembr. 1281*, 139–149.
(25) Li, S., Tseng, W. C., Stolz, D. B., Wu, S. P., Watkins, S. C., and Huang, L. (1999) Dynamic changes in the characteristics of cationic lipidic vectors after exposure to mouse serum: implications for intravenous lipofection. *Gene Ther. 6*, 585–594.
(26) McLean, J. W., Fox, E. A., Baluk, P., Bolton, P. B., Haskell, A., Pearlman, R., Thurston, G., Umemoto, E. Y., and McDonald, D. M. (1997) Organ-specific endothelial cell uptake of cationic liposome-DNA complexes in mice. *Am. J. Physiol. 273*, H387–404.
(27) van de Water, F. M., Boerman, O. C., Wouterse, A. C., Peters, J. G., Russel, F. G., and Masereeuw, R. (2006) Intravenously administered short interfering RNA accumulates in the kidney and selectively suppresses gene function in renal proximal tubules. *Drug Metab. Dispos. 34*, 1393–1397.
(28) Lendvai, G., Velikyan, I., Bergstrom, M., Estrada, S., Laryea, D., Valila, M., Salomaki, S., Langstrom, B., and Roivainen, A. (2005) Biodistribution of 68Ga-labelled phosphodiester, phosphorothioate, and 2′-O-methyl phosphodiester oligonucleotides in normal rats. *Eur. J. Pharm. Sci. 26*, 26–38.
(29) Braasch, D. A., Paroo, Z., Constantinescu, A., Ren, G., Oz, O. K., Mason, R. P., and Corey, D. R. (2004) Biodistribution of phosphodiester and phosphorothioate siRNA. *Bioorg. Med. Chem. Lett. 14*, 1139–1143.
(30) Liu, N., Ding, H., Vanderheyden, J. L., Zhu, Z., and Zhang, Y. (2007) Radiolabeling small RNA with technetium-99m for visualizing cellular delivery and mouse biodistribution. *Nucl. Med. Biol. 34*, 399–404.

BC9005267

International Journal of Pharmaceutics 392 (2010) 218–223

Contents lists available at ScienceDirect

International Journal of Pharmaceutics

journal homepage: www.elsevier.com/locate/ijpharm

Pharmaceutical Nanotechnology

T cell-independent B cell response is responsible for ABC phenomenon induced by repeated injection of PEGylated liposomes

Hiroyuki Koide[a], Tomohiro Asai[a], Kentaro Hatanaka[a], Shuji Akai[b], Takayuki Ishii[a], Eriya Kenjo[a], Tatsuhiro Ishida[c], Hiroshi Kiwada[c], Hideo Tsukada[d], Naoto Oku[a,*]

[a] Department of Medical Biochemistry and Global COE Program, Graduate School of Pharmaceutical Sciences, University of Shizuoka, 52-1 Yada, Suruga-ku, Shizuoka 422-8526, Japan
[b] Department of Synthetic Organic Chemistry, Graduate School of Pharmaceutical Sciences, University of Shizuoka, 52-1 Yada, Suruga-ku, Shizuoka 422-8526, Japan
[c] Department of Pharmacokinetics and Biopharmaceutics, Institute of Health Biosciences, The University of Tokushima, 1-78-1, Sho-machi, Tokushima 770-8505, Japan
[d] Central Research Laboratory, Hamamatsu Photonics K.K., Hamamatsu, Shizuoka, Japan

ARTICLE INFO

Article history:
Received 9 December 2009
Received in revised form 8 February 2010
Accepted 8 March 2010
Available online 21 March 2010

Keywords:
Polyethylene glycol
Liposome
Accelerated blood clearance
Thymus-independent type 2 antigen
Nanocarriers

ABSTRACT

Repeated injection of polyethyleneglycol-modified (PEGylated) liposomes causes a rapid clearance of them from the bloodstream, this phenomenon is called accelerated blood clearance (ABC). In the present study, we focused on the immune system responsible for the ABC phenomenon. PEGylated liposomes were preadministered to BALB/c mice and [^{3}H]-labeled ones were then administered to them 3 days after the preadministration. Consistent with our previous results, the preadministration with PEGylated liposomes triggered the rapid clearance of [^{3}H]-labeled PEGylated liposomes from the bloodstream, but that with PEGylated liposomes encapsulating doxorubicin (Dox) did not. In addition, we found that the ABC phenomenon was observed when a mixture of free Dox and PEGylated liposomes was preadministered. These data indicate that immune cells responsible for the ABC phenomenon might be selectively damaged by the Dox encapsulated in PEGylated liposomes. The ABC phenomenon was also observed in BALB/c *nu/nu* mice, but not in BALB/c SCID mice. The amount of anti-PEG IgM antibody induced by the stimulation with the PEGylated liposomes was significantly increased in the BALB/c *nu/nu* mice, but not in the BALB/c SCID ones. These data indicate that a T cell-independent B cell response would play a significant role in the ABC phenomenon. Furthermore, the present study suggests that PEGylated liposomes might be recognized by B cells as a thymus-independent type 2 (TI-2) antigen. The present study provides important information for the future development of liposomal medicines.

1. Introduction

PEGylated liposomes have been widely investigated as drug carriers and gene delivery systems. PEG forms a water shell on the liposomal surface and provides a steric barrier to the liposomes for avoiding interactions with plasma proteins, resulting in escape from trapping by the reticuloendothelial system (Lasic et al., 1991; Torchilin et al., 1994; Van Rooijen and Van Nieuwmegen, 1980). Therefore, PEGylated liposomes have the property of long circulation and are useful for drug delivery to tumors and inflamed sites, resulting in improving the therapeutic indices of encapsulated drugs (Allen, 1994). As a representative example of liposomal drugs, Doxil® has been used clinically. Doxil® is PEGylated liposomes encapsulating doxorubicin, which is used for reducing side effects of Dox such as cardiotoxicity and for enhancing its anticancer activity through enhanced permeability and retention (EPR) effect (Berry et al., 1998; Maeda et al., 2000; Muggia, 1999). On the other hand, we and others have found that a repeat injection of PEGylated liposomes into certain animals such as mice, rats and rhesus monkey triggers the rapid clearance of the second dose through their accumulation in the liver (Dams et al., 2000; Ishida et al., 2003a,b). This phenomenon, called as the accelerated blood clearance (ABC) phenomenon, is expected to have a considerable impact on the clinical use of liposomal formulations (Dams et al., 2000; Ishida et al., 2003a,b). A previous study of ours indicated that when rats were pretreated with a high dose (more than 5 μmol phospholipids/kg) of PEGylated liposomes, the induction of the ABC phenomenon was weakened. However, when rats were pretreated with a low concentration of them (1 μmol phospholipids/kg), the phenomenon was strongly induced (Ishida et al., 2006a,b,c). This phenomenon was widely observed even if the content of PEG lipid in liposomes or the length of the

Abbreviations: ABC phenomenon, accelerated blood clearance phenomenon; [^{3}H]-CHE, [^{3}H] cholesterylhexadecyl ether; MPEG-DSPE, 1,2-distearoyl-sn-glycero-3-phosphoethanolamine-n-[methoxy(polyethylene glycol)-2000]; MPS, mononuclear phagocyte system; PEGylated liposomes, polyethylene glycol-modified liposomes.

* Corresponding author. Tel.: +81 54 264 5701; fax: +81 54 264 5705.
E-mail address: oku@u-shizuoka-ken.ac.jp (N. Oku).

0378-5173/$ – see front matter © 2010 Elsevier B.V. All rights reserved.
doi:10.1016/j.ijpharm.2010.03.022

PEG chain was varied. In fact, both methoxy(polyethyleneglycol)-2000-distearoylphosphatidylethanolamine (mPEG$_{2000}$-DSPE) and mPEG$_{5000}$-DSPE induced the phenomenon, and the concentration of mPEG$_{2000}$-DSPE in the first-dose PEGylated liposomes did not affect on the induction of the phenomenon (Ishida et al., 2005). In an earlier study, we also demonstrated that the spleen could play a key role in induction of the ABC phenomenon via secretion of anti-PEG IgM antibody by splenic B cells (Ishida et al., 2006a,b,c). Anti-PEG IgM antibody was gradually secreted by the administration of PEGylated liposomes and bound to the liposomes in the secondary injection, resulting in the rapid clearance of them from the bloodstream via complement activation (Ishida et al., 2005, 2007). Furthermore, the ABC phenomenon was triggered by preadministration with not only PEGylated liposomes but also polymeric micelles having PEG chains (Koide et al., 2008).

Our recent reports showed that the administration of Dox encapsulated in PEGylated liposomes (PEG–Dox) did not alter the pharmacokinetics of PEGylated liposomes injected as the test-dose (Ishida et al., 2006a,b,c; Laverman et al., 2001). In the present study, we firstly focused on the effect of Dox in the liposomes on the immune cells responsible for the ABC phenomenon. Then, we investigated the immune mechanism involved in this phenomenon.

2. Materials and methods

2.1. Materials

Dipalmitoylphosphatidylcholine (DPPC), cholesterol (Cho), and distearoylphosphoethanolamine-*N*-[methoxy(polyethyleneglycol)-2000] (mMPEG-DSPE) were kindly donated by Nippon Fine Chemical Co., Ltd. (Takasago, Hyogo, Japan). [^{3}H]cholesterylhexadecyl ether ([^{3}H]-CHE) was purchased from Amersham Pharmacia (Buckinghamshire, UK). All other reagents were analytical grade.

2.2. Animal

Five-week-old male BALB/c and BALB/c *nu/nu* mice were purchased from Japan SLC Inc. (Shizuoka, Japan). Five-week-old male CB17/Icr-Prkdc^{scid}/CrlCrlj (BALB/c SCID) mice were purchased from Charles River Japan, Inc. (Kanagawa, Japan). The animals were cared according to the animal facility guidelines of the University of Shizuoka.

2.3. Preparation of liposomes

PEGylated liposomes composed of DPPC and Cho with mPEG-DSPE (10:5:1 as a molar ratio) were prepared as described previously (Maeda et al., 2004). In brief, lipids dissolved in chloroform were evaporated to obtain a thin lipid film. Then, liposomes were formed by hydration with 10 mM phosphate-buffered 0.3 M sucrose solution and then sized by 5-times extrusion through a polycarbonate membrane filter with 100 nm pores (Nucleopore, Maidstone, UK). For a biodistribution study, a trace amount of [^{3}H]-CHE (74 kBq/mouse) was added to the initial chloroform solution. Dox-encapsulated liposomes were prepared by a modification of the remote loading method as described previously (Oku et al., 1994). The concentration of Dox was determined by its absorbance at 484 nm. The particle size of PEGylated liposomes was measured by use of a Zetasizer Nano ZS (MALVERN, Worcestershire, UK) after dilution of the liposomes with PBS, pH 7.4.

2.4. Biodistribution of PEGylated liposomes

Mice received an intravenous injection of PEGylated liposomes (2.0 μmol phospholipids/kg), PEG–Dox liposomes (1 mg/kg as a Dox dosage), a mixture of free Dox (1 mg/kg) and "empty" PEGylated liposomes or PBS. Three days later, [^{3}H]-labeled PEGylated liposomes (5.0 μmol phospholipids/kg) were administered to the mice via a tail vein. Twenty-four hours after the second administration, these mice were sacrificed under deep anesthesia for the collection of blood. Then, the blood was heparinized and separated by centrifugation (700 × *g*, 15 min, 4 °C) to obtain the plasma. After the mice had been bled from the carotid artery, their heart, lungs, liver, spleen, and kidneys were removed and weighed. The radioactivity in plasma and each organ was determined with a liquid scintillation counter (LSC-3100, Aloka, Tokyo, Japan). Tissue distribution data were presented as % dose per wet tissue. The total radioactivity in the plasma was calculated based on the average body weight of the mice, where the average plasma volume was assumed to be 4.27% of the body weight based on the data on total blood volume.

2.5. Detection of anti-PEG IgM antibody

Mice were intravenously injected with PEGylated liposomes (2.0 μmol phospholipids/kg), PEG–Dox liposomes (1 mg/kg as a Dox dosage), a mixture of free Dox (1 mg/kg) and "empty" PEGylated liposomes or PBS. Three days later, these mice were sacrificed and their blood was withdrawn. Serum was collected after centrifugation (700 × *g*, 15 min, 4 °C). To prepare the ELISA plates, 10 μg of mPEG-DSPE in 20 μL ethanol was added to 96-well plates (Nunc, Roskilde, Denmark). Then, the plates were air dried for 2 h to complete dryness and subsequently blocked with 10% fetal bovine serum (FBS, Sigma–Aldrich, St. Louis, MO) in PBS for 1 h. The diluted serum samples (100 μl) were added to the plates, incubated for 1 h, and washed 5 times with 1% FBS-PBS. Antibodies bound to mPEG-DSPE were detected with HRP-conjugated goat anti-mouse IgM antibody (Bethyl Laboratories, TX, USA). After incubation with the anti-IgM antibody for 1 h, each well was washed 5 times with 1% FBS-PBS. The coloration was initiated by the addition of *o*-phenylene diamine dihydrochloride (Sigma, St. Louis, MO, USA) that had been diluted with distilled water. After a 15-min incubation, the reaction was stopped by adding 100 μL of 2 M H_2SO_4, and the absorbance was recorded at 490 nm.

2.6. Synthesis of a positron emitter-labeled probe

The synthesis of 1-[^{18}F] fluoro-3,6-dioxatetracosane (SteP2) was prepared as described previously (Urakami et al., 2007). Briefly, [^{18}F] fluoride was produced with a cyclotron (HM-18, Sumitomo Heavy Industries, Tokyo, Japan) at Hamamatsu Photonics PET Center, and the labeled compound was synthesized from the precursor.

2.7. [^{18}F]-Labeling of PEGylated liposomes

[^{18}F]-Labeling of PEGylated liposomes were performed by a solid-phase transition (SophT) method (Urakami et al., 2007). About 100 MBq of [^{18}F]-SteP2 in ethanol solution was transferred to a glass test tube, and the solvent was removed completely at 90 °C with a flow of helium gas. PEGylated liposomes were added to the tube and incubated at 37 °C for 15 min with 5-s mixing by use of a vortex stirrer every 3 min. After the incubation, the PEGylated liposomes were centrifuged at 100,000 × *g* for 15 min (Beckman, Fullerton, CA, USA), and the supernatant was transferred to a new tube. Radioactivity of supernatant, precipitate, and original tube for labeling was measured with a curiemeter (IGC-3, Aloka, Tokyo, Japan) to calculate the labeling efficiency.

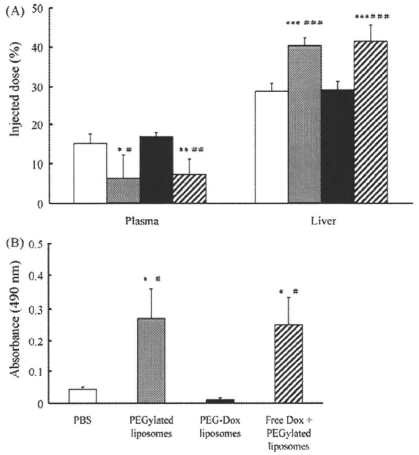

Fig. 1. Abolishment of the ABC phenomenon with Dox encapsulated in PEGylated liposomes. BALB/c mice were intravenously injected with PBS, PEGylated liposomes, PEG–Dox liposomes or a mixture of free Dox and "empty" PEGylated liposomes. (A) Biodistribution of the test-dose ^{3}H-labeled PEGylated liposomes: 3 days after the pretreatment, ^{3}H-labeled PEGylated liposomes were intravenously injected into these mice (5 μmol DPPC dosage/kg). Twenty-four hours after the second injection, the mice were sacrificed, and the radioactivity in the plasma and each organ (only liver data shown) was determined. Data ($n=5$) are presented as a percentage of the injected dose per tissue and S.D. and (B) anti-PEG IgM in the serum collected at day 3 after the pretreatment. Each value represents the mean ± S.D. of 3 separate experiments. Data are presented for PBS (open bar), PEGylated liposomes (gray bar), PEG–Dox liposomes (closed bar), and a mixture of free Dox and PEGylated liposomes (hatched bar). Significant differences: $^{*}p<0.05$, $^{**}p<0.01$, and $^{***}p<0.001$ *vs.* PBS; $^{\#}p<0.05$, $^{\#\#}p<0.01$, and $^{\#\#\#}p<0.001$ *vs.* PEG–Dox.

2.8. Imaging of [^{18}F]-labeled PEGylated liposomes by planar positron imaging system (PPIS)

Biodistribution of [^{18}F]-labeled PEGylated liposomes was determined with a positron planar imaging system (PPIS, Hamamatsu Photonics, Shizuoka, Japan). Mice anesthetized with chloral hydrate were positioned prone on an acrylic plate and placed between the 2 opposing detectors. An [^{18}F]-labeled sample at the dose of 2.5 MBq was intravenously injected into a mouse via a tail vein. The data were acquired with a 1-min time frame interval for 60 min, and 2 summation images were created every 30 min.

2.9. Statistics

Variance in a group was evaluated by using Student's *t*-test.

3. Results

3.1. Abolishment of ABC phenomenon by preadministration with Dox encapsulated in PEGylated liposomes

Mice were intravenously injected with PEGylated liposomes, PEG–Dox liposomes, a mixture of free Dox and "empty" PEGylated liposomes, or PBS for preconditioning. Three days later, these mice were administered PEGylated liposomes labeled with [^{3}H]-CHE as the test-dose. Fig. 1A shows the biodistribution of the test-dose PEGylated liposomes 24 h after the injection. Pretreatment with the PEG–Dox liposomes did not alter the plasma level or hepatic uptake of the test-dose compared with that with PBS. However, in case of pretreatment with the mixture of free Dox and "empty" PEGylated liposomes, the amount of test-dose significantly decreased in the plasma and significantly increased in the liver. The biodistribution pattern for this group was similar to that for the PEGylated liposome-injected group. The accumulation of the test-dose in other organs did not show significant differences among all groups tested (data not shown). Next, anti-PEG IgM antibody secretion was examined 3 days after the preconditioning (Fig. 1B). When either PEGylated liposomes or the mixture of free Dox and PEGylated liposomes were administered, production of anti-PEG IgM antibody was increased about 6-fold compared with the baseline level obtained for the PBS group. Whereas, when the mice were injected with the PEG–Dox liposomes, the production did not increase at all.

3.2. Imaging of biodistribution of PEGylated liposomes with PPIS

To assess the ABC phenomenon non-invasively, we next examined the change in the real-time distribution of PEGylated liposomes by use of PPIS. [^{18}F]-Labeled PEGylated liposomes were intravenously administered to the mice that had been pretreated with PEGylated liposomes, PEG–Dox liposomes or PBS 3 days before, and the biodistribution was imaged (Fig. 2). The biodistribution of [^{18}F]-labeled PEGylated liposomes was imaged for 60 min, and the images were integrated into 1–30 and 31–60 min composite images. In the 1–30 min image, weak [^{18}F] signals were observed in the lung, spleen, kidney and bladder, and strong signals were detected in the liver, particularly in the mice pretreated with PEGylated liposomes. In the 31–60 min image, these signals were reduced in the lung, spleen, kidney and liver in the groups pretreated with PBS or PEG–Dox, and were significantly increased in the bladder in both groups. However, relatively strong signals remained in the group pretreated with the PEGylated liposomes.

3.3. Induction of ABC phenomenon in BALB/c nu/nu mice

BALB/c *nu/nu* (T cell-deficient) mice were preadministered PBS, PEGylated liposomes or PEG–Dox ones to clarify the role of T cells in the induction of the ABC phenomenon. In the mice pretreated with PEGylated liposomes, the amount of PEGylated liposomes significantly decreased in the plasma and significantly increased in the liver. This indicates that the ABC phenomenon was induced in BALB/c *nu/nu* mice (Fig. 3A). Consistent with the data for BALB/c mice, the pretreatment with PEG–Dox liposomes did not alter the pharmacokinetics of the test-dose PEGylated liposomes in these BALB/c *nu/nu* mice. The anti-PEG IgM antibody production was significantly increased in the mice pretreated with the PEGylated but not PEG–Dox liposomes (Fig. 3B). All results obtained for the BALB/c *nu/nu* mice were similar to those obtained for the BALB/c ones.

3.4. Significant role of B cells in the ABC phenomenon

Since T cells did not seem to be involved in the induction of the ABC phenomenon, we next determined the function of B cells in this phenomenon by using SCID mice, which are known to be deficient in both T and B cells. The biodistribution of test-dose PEGylated liposomes in BALB/c SCID mice was determined. As a result, any preadministrations (PEGylated liposomes, PEG–Dox liposomes, or PBS) did not alter the pharmacokinetics of the test-dose PEGylated liposomes. These results indicate that the ABC phenomenon was not induced in BALB/c SCID mice and that B cells play an important role in the induction of the ABC phenomenon (Fig. 4A). In addition, anti-PEG IgM antibody was not detected in any of the BALB/c SCID groups (Fig. 4B).

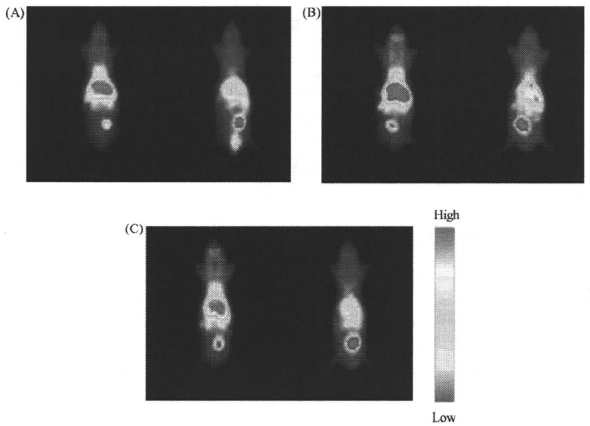

Fig. 2. Imaging of biodistribution of PEGylated liposomes with PPIS. Whole-body imaging of biodistribution of [^{18}F]-labeled PEGylated liposomes in BALB/c mice pretreated with PBS (A), PEGylated liposomes (B), or PEG–Dox liposomes (C) was performed by use of PPIS. Data were integrated into 1–30 (left image) or 31–60 min (right image) periods following the injection of [^{18}F]-labeled PEGylated liposomes.

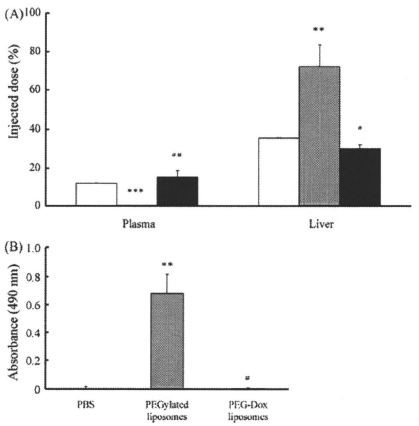

Fig. 3. Induction of the ABC phenomenon in BALB/c *nu/nu* mice. BALB/c *nu/nu* mice were intravenously injected with PBS, PEGylated liposomes or PEG–Dox liposomes. (A) Biodistribution of the test-dose ^{3}H-labeled PEGylated liposomes: 3 days after the pretreatment, ^{3}H-labeled PEGylated liposomes were intravenously injected into these mice (5 μmol DPPC dosage/kg). Twenty-four hours after the second injection, the mice were sacrificed, and the radioactivity in the plasma and each organ (only liver data shown) was determined. Data ($n = 5$) are presented as a percentage of the injected dose per tissue and S.D. and (B) anti-PEG IgM in the serum collected at day 3 after the pretreatment. Each value represents the mean ± S.D. of 3 separate experiments. Data are presented for PBS (open bar), PEGylated liposomes (gray bar), and PEG–Dox liposomes (closed bar). Significant differences: $^{**}p < 0.01$ and $^{***}p < 0.001$ *vs.* PBS; $^{\#\#}p < 0.01$ and $^{\#}p < 0.001$ *vs.* PEGylated liposomes.

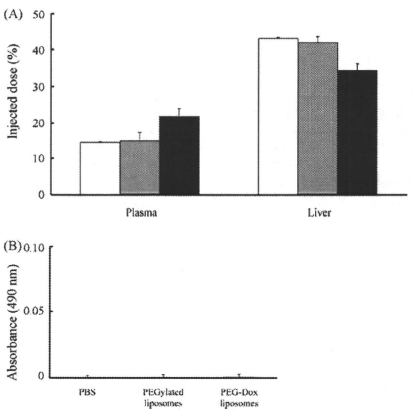

Fig. 4. No induction of the ABC phenomenon in BALB/c SCID mice. BALB/c SCID mice were intravenously injected with PBS, PEGylated liposomes or PEG–Dox liposomes. (A) Biodistribution of the test-dose ^{3}H-labeled PEGylated liposomes: 3 days after the pretreatment, ^{3}H-labeled PEGylated liposomes were administered via a tail vein (5 μmol DPPC dosage/kg). Twenty-four hours after the second injection, these mice were sacrificed; and the radioactivity in the plasma and each organ was then determined. Data ($n = 5$) are presented as a percentage of the injected dose per tissue and S.D. and (B) anti-PEG IgM in the serum collected at day 3 after the pretreatment. Each value represents the mean ± S.D. of 3 separate experiments. Data are presented for PBS (open bar), PEGylated liposomes (gray bar), and PEG–Dox (closed bar).

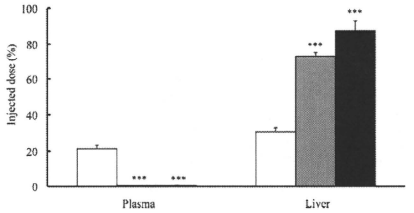

Fig. 5. Induction of the ABC phenomenon with non-PEGylated liposomes. BALB/c mice were intravenously injected with PBS, PEGylated liposomes, or non-PEGylated liposomes. Three days after pretreatment, ^{3}H-labeled PEGylated liposomes were administered via a tail vein. Twenty-four hours after the second injection, these mice were sacrificed; and the radioactivity in the plasma and each organ was then determined ($n=5$). Data are presented as a percentage of the injected dose per tissue and S.D. Data are presented for PBS (open bar), PEGylated liposomes (gray bar), and non-PEGylated liposomes (closed bar), respectively. Significant differences: $^{***}p<0.001$ *vs.* PBS.

3.5. Low specificity in the induction of the ABC phenomenon

We next focused on the specificity in the induction of the ABC phenomenon since T cell-independent B cell response against thymus-independent type 2 (TI-2) antigen might trigger this phenomenon. To elucidate the specificity in the induction of the ABC phenomenon, we preadministered non-PEGylated liposomes to BALB/c mice, and then studied the biodistribution of the test-dose PEGylated liposomes. As shown in Fig. 5, the hepatic uptake and the clearance from bloodstream of the test-dose PEGylated liposomes were increased dramatically in the mice pretreated with non-PEGylated liposomes, as in the case of pretreatment with PEGylated liposomes. This indicates that the ABC phenomenon was thus induced regardless of modification of the liposomes with PEG chains.

3.6. Time-dependency of anti-PEG IgM antibody production

We next determined the time-dependency of the production of anti-PEG IgM antibody in BALB/c mice. The amount of anti-PEG IgM antibody was determined at days 1, 3, 7, 11, 14, 21 and 27 after pretreatment with PEGylated liposomes, PEG–Dox liposomes, or PBS. Anti-PEG IgM antibody production reached maximum level about 3 days after the administration of PEGylated liposomes (Fig. 6). This transient increase in IgM antibody like T cell-independent B cell response was observed in this experiment. On the contrary, the PBS and PEG–Dox liposomes groups showed little production of anti-PEG IgM antibody.

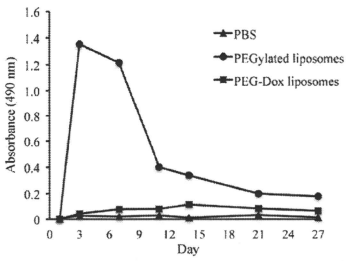

Fig. 6. Time-course of anti-PEG IgM antibody production. BALB/c mice were intravenously injected with PBS, PEGylated liposomes or PEG–Dox liposomes. At days 1, 3, 7, 11, 14, 21, and 27 after the injection, serum samples were collected. Anti-PEG IgM antibody was then detected by ELISA.

4. Discussion

The ABC phenomenon implies caution about the pharmacokinetics of nanoparticles in the case of repeated injection of nanomedicines, especially in the clinical setting. Thus, elucidating the mechanism of the ABC phenomenon is important for the development of DDS (drug delivery system) drugs. In this study, we determined the biodistribution of test-dose PEGylated liposomes in mice preadministered PEG–Dox liposomes or a mixture of free Dox and "empty" PEGylated liposomes. We and Laverman et al. previously reported that the ABC phenomenon was not induced when the rats were pretreated with PEG–Dox liposomes (Ishida et al., 2006a,b,c; Laverman et al., 2001). These reports indicated that preadministration of PEG–Dox liposomes could abolish the induction of the ABC phenomenon, although the effect of the mixture of free Dox and "empty" PEGylated liposomes has not been clarified. The production of anti-PEG IgM antibody was increased by the administration of the mixture of free Dox and "empty" PEGylated liposomes in a manner similar to that of PEGylated liposomes, but no increase was seen with PEG–Dox liposomes. These data suggest the importance of Dox delivery to immune cells by PEGylated liposomes, and indicate that Dox encapsulated in the liposomes was delivered to the immune cells responsible for the ABC phenomenon. And then, Dox that had been taken up into the immune cells could induce apoptosis of them, resulting in no induction of the IgM antibody against PEGylated liposomes and ABC phenomenon. In general, free Dox causes adverse reactions such as leucopenia and cardiotoxicity. Liposomal Dox was developed to reduce these side effects, which could significantly increase the tolerable dosage (O'brien et al., 2004). If the induction of the ABC phenomenon was canceled by a non-specific effect of Dox, the mixture of free Dox and "empty" PEGylated liposomes would have abolished the induction of the phenomenon. Accordingly, we conclude that the encapsulation of cytotoxic agents in PEGylated liposomes prevents the induction of the ABC phenomenon.

The ABC phenomenon was observed in the BALB/c *nu/nu* mice, but not in the BALB/c SCID mice. In addition, production of anti-PEG IgM antibody was increased by the injection of PEGylated liposomes in BALB/c *nu/nu* mice but not in BALB/c SCID mice at all. These results suggest that the induction of ABC phenomenon is independent of the T cells, but dependent on B cells. On the other hand, the phenomenon was also induced by the preadministration of non-PEGylated liposomes, suggesting that the specificity of the IgM antibody would be comparatively low. In this point, we previously reported that the administration of PEGylated liposomes triggered IgM antibody production against both PEG moieties and lipid moieties in rats, although the reactivity of IgM antibody against the latter was not so high (Wang et al., 2007). Anti-PEG IgM antibody produced by preadministration of PEGylated liposomes was transiently increased and then decreased rapidly. These data suggest that PEGylated liposomes might be recognized as a TI-2 antigen.

In general, most antigens in the natural world are T cell-dependent antigen. In the immune response to them, naïve B cells can differentiate into immunoglobulin-secreting cells or they can seed a germinal center and develop into memory B cells after exposure to a T cell-dependent antigen (Ahmed and Gray, 1996; Liu et al., 1988, 1991). However, there are other type antigens which are composed of repetitive structures such as polysaccharides or lipopolysaccharide derived from bacteria and belong to the TI-2 antigen category. These antigens activate B cells, which then produce antibodies such as IgM and IgG without the interaction with

helper T cells; and these IgM antibodies tend to have low affinity (Beringue et al., 2000). TI-2 responses are characterized by early B cell proliferation in all splenic compartments and differentiation into antibody-producing plasma cells starting at day 3 after immunization, but the number of plasma cells falls markedly during the second week after immunization (Garcia De Vinuesa et al., 1999). These TI-2 antigens induce only limited isotype switching and do not induce memory B cells (Beringue et al., 2000). In addition, B cells respond against TI-2 antigens and profoundly participate in the response of complements (Zandvoort and Timens, 2002). It is therefore considered that when PEGylated liposomes enter into the bloodstream, complement components may bind to the liposomal surface and activate B cells to secrete IgM antibodies such as anti-PEG IgM antibody. Marginal zone B (MZ-B) cells in the spleen and B-1B cells in the intraperitoneal cavity play a central role in the immune response against TI-2 antigen (Martin and Kearney, 2002). Since we have already reported that the phenomenon was not induced in rats that had had their spleens removed (Ishida et al., 2006a,b,c), we hypothesize that MZ-B cells recognize PEGylated liposomes as a TI-2 antigen and secrete anti-PEG IgM antibody. It appears that anti-PEG IgM antibody binds to the test-dose PEGylated liposomes and makes complexes with complement components. Then, these complexes accumulate in the liver, resulting in the rapid clearance of PEGylated liposomes.

Our present findings strongly suggest that PEGylated liposomes and conventional liposomes without PEG modification are recognized as TI-2 antigens and that the induction of the ABC phenomenon is related to a T cell-independent B cell response.

5. Conclusion

This study revealed that the ABC phenomenon occurred in BALB/c *nu/nu* mice, but not in BALB/c SCID mice. Anti-IgM antibody production, possibly derived from a T cell-independent B cell response, would be essential for the induction of the phenomenon. We anticipate that the elucidation of the ABC phenomenon will be helpful for the development of future DDS formulations.

Acknowledgments

This research was supported by global COE program. We thank Philip Hawke at the University of Shizuoka for helpful advice in writing the manuscript.

References

Ahmed, R., Gray, D., 1996. Immunological memory and protective immunity: understanding their relation. Science 272, 54–60.

Allen, T.M., 1994. Long-circulating (sterically stabilized) liposomes for targeted drug delivery. Trends Pharmacol. Sci. 15, 215–220.

Beringue, V., Demoy, M., Lasmezas, C.I., Gouritin, B., Weingarten, C., Deslys, J.P., Andreux, J.P., Couvreur, P., Dormont, D., 2000. Role of spleen macrophages in the clearance of scrapie agent early in pathogenesis. J. Pathol. 190, 495–502.

Berry, G., Billingham, M., Alderman, E., Richardson, P., Torti, F., Lum, B., Patek, A., Martin, F.J., 1998. The use of cardiac biopsy to demonstrate reduced cardiotoxicity in AIDS Kaposi's sarcoma patients treated with pegylated liposomal doxorubicin. Ann. Oncol. 9, 711–716.

Dams, E.T., Laverman, P., Oyen, W.J., Storm, G., Scherphof, G.L., Van Der Meer, J.W., Corstens, F.H., Boerman, O.C., 2000. Accelerated blood clearance and altered biodistribution of repeated injections of sterically stabilized liposomes. J. Pharmacol. Exp. Ther. 292, 1071–1079.

Garcia De Vinuesa, C., O'leary, P., Sze, D.M., Toellner, K.M., Maclennan, I.C., 1999. T-independent type 2 antigens induce B cell proliferation in multiple splenic sites, but exponential growth is confined to extrafollicular foci. Eur. J. Immunol. 29, 1314–1323.

Ishida, T., Atobe, K., Wang, X., Kiwada, H., 2006a. Accelerated blood clearance of PEGylated liposomes upon repeated injections: effect of doxorubicin-encapsulation and high-dose first injection. J. Control. Release 115, 251–258.

Ishida, T., Harada, M., Wang, X.Y., Ichihara, M., Irimura, K., Kiwada, H., 2005. Accelerated blood clearance of PEGylated liposomes following preceding liposome injection: effects of lipid dose and PEG surface-density and chain length of the first-dose liposomes. J. Control. Release 105, 305–317.

Ishida, T., Ichihara, M., Wang, X., Kiwada, H., 2006b. Spleen plays an important role in the induction of accelerated blood clearance of PEGylated liposomes. J. Control. Release 115, 243–250.

Ishida, T., Ichihara, M., Wang, X., Yamamoto, K., Kimura, J., Majima, E., Kiwada, H., 2006c. Injection of PEGylated liposomes in rats elicits PEG-specific IgM, which is responsible for rapid elimination of a second dose of PEGylated liposomes. J. Control. Release 112, 15–25.

Ishida, T., Maeda, R., Ichihara, M., Irimura, K., Kiwada, H., 2003a. Accelerated clearance of PEGylated liposomes in rats after repeated injections. J. Control. Release 88, 35–42.

Ishida, T., Masuda, K., Ichikawa, T., Ichihara, M., Irimura, K., Kiwada, H., 2003b. Accelerated clearance of a second injection of PEGylated liposomes in mice. Int. J. Pharm. 255, 167–174.

Ishida, T., Wang, X., Shimizu, T., Nawata, K., Kiwada, H., 2007. PEGylated liposomes elicit an anti-PEG IgM response in a T cell-independent manner. J. Control. Release 122, 349–355.

Koide, H., Asai, T., Hatanaka, K., Urakami, T., Ishii, T., Kenjo, E., Nishihara, M., Yokoyama, M., Ishida, T., Kiwada, H., Oku, N., 2008. Particle size-dependent triggering of accelerated blood clearance phenomenon. Int. J. Pharm. 362, 197–200.

Lasic, D.D., Martin, F.J., Gabizon, A., Huang, S.K., Papahadjopoulos, D., 1991. Sterically stabilized liposomes: a hypothesis on the molecular origin of the extended circulation times. Biochim. Biophys. Acta 1070, 187–192.

Laverman, P., Carstens, M.G., Boerman, O.C., Dams, E.T., Oyen, W.J., Van Rooijen, N., Corstens, F.H., Storm, G., 2001. Factors affecting the accelerated blood clearance of polyethylene glycol-liposomes upon repeated injection. J. Pharmacol. Exp. Ther. 298, 607–612.

Liu, Y.J., Oldfield, S., Maclennan, I.C., 1988. Memory B cells in T cell-dependent antibody responses colonize the splenic marginal zones. Eur. J. Immunol. 18, 355–362.

Liu, Y.J., Zhang, J., Lane, P.J., Chan, E.Y., Maclennan, I.C., 1991. Sites of specific B cell activation in primary and secondary responses to T cell-dependent and T cell-independent antigens. Eur. J. Immunol. 21, 2951–2962.

Maeda, H., Wu, J., Sawa, T., Matsumura, Y., Hori, K., 2000. Tumor vascular permeability and the EPR effect in macromolecular therapeutics: a review. J. Control. Release 65, 271–284.

Maeda, N., Takeuchi, Y., Takada, M., Sadzuka, Y., Namba, Y., Oku, N., 2004. Anti-neovascular therapy by use of tumor neovasculature-targeted long-circulating liposome. J. Control. Release 100, 41–52.

Martin, F., Kearney, J.F., 2002. Marginal-zone B cells. Nat. Rev. Immunol. 2, 323–335.

Muggia, F.M., 1999. Doxorubicin-polymer conjugates: further demonstration of the concept of enhanced permeability and retention. Clin. Cancer Res. 5, 7–8.

O'brien, M., Wigler, N., Inbar, M., Rosso, R., Grischke, E., Santoro, A., Catane, R., Kieback, D., Tomczak, P., Ackland, S., Orlandi, F., Mellars, L., Alland, L., Tendler, C., Group Caelyx Breast Cancer Study, 2004. Reduced cardiotoxicity and comparable efficacy in a phase III trial of pegylated liposomal doxorubicin HCl (CAELYX/Doxil) versus conventional doxorubicin for first-line treatment of metastatic breast cancer. Ann. Oncol. 15, 440–449.

Oku, N., Doi, K., Namba, Y., Okada, S., 1994. Therapeutic effect of adriamycin encapsulated in long-circulating liposomes on Meth-A-sarcoma-bearing mice. Int. J. Cancer 58, 415–419.

Torchilin, V.P., Omelyanenko, V.G., Papisov, M.I., Bogdanov Jr., A.A., Trubetskoy, V.S., Herron, J.N., Gentry, C.A., 1994. Poly(ethylene glycol) on the liposome surface: on the mechanism of polymer-coated liposome longevity. Biochim. Biophys. Acta 1195, 11–20.

Urakami, T., Akai, S., Katayama, Y., Harada, N., Tsukada, H., Oku, N., 2007. Novel amphiphilic probes for [18F]-radiolabeling preformed liposomes and determination of liposomal trafficking by positron emission tomography. J. Med. Chem. 50, 6454–6457.

Van Rooijen, N., Van Nieuwmegen, R., 1980. Liposomes in immunology: multilamellar phosphatidylcholine liposomes as a simple, biodegradable and harmless adjuvant without any immunogenic activity of its own. Immunol. Commun. 9, 243–256.

Wang, X., Ishida, T., Kiwada, H., 2007. Anti-PEG IgM elicited by injection of liposomes is involved in the enhanced blood clearance of a subsequent dose of PEGylated liposomes. J. Control. Release 119, 236–244.

Zandvoort, A., Timens, W., 2002. The dual function of the splenic marginal zone: essential for initiation of anti-TI-2 responses but also vital in the general first-line defense against blood-borne antigens. Clin. Exp. Immunol. 130, 4–11.

BRAIN RESEARCH 1321 (2010) 164–168

available at www.sciencedirect.com

ScienceDirect

www.elsevier.com/locate/brainres

BRAIN RESEARCH

Research Report

Accumulation of macromolecules in brain parenchyma in acute phase of cerebral infarction/reperfusion

*Takayuki Ishii, Tomohiro Asai, Takeo Urakami, Naoto Oku**

Department of Medical Biochemistry and Global COE, School of Pharmaceutical Sciences, University of Shizuoka, 52-1 Yada, Suruga-ku, Shizuoka 422-8526, Japan

ARTICLE INFO

Article history:
Accepted 13 January 2010
Available online 21 January 2010

Keywords:
Stroke
Reperfusion injury
BBB
t-MCAO
Macromolecule

ABSTRACT

Ischemia–reperfusion injury is induced by recovery of blood flow after ischemia. This phenomenon is a main cause of ischemic brain injury. The integrity of the blood–brain barrier (BBB) fails after cerebral ischemia and reperfusion. Further elucidation of this phenomenon promotes to develop treatment strategies for ischemia–reperfusion injury. In the present study, we attempted to examine the time-dependent change of ischemia–reperfusion injury in relation to BBB disorders at acute phase in a transient middle cerebral artery occlusion (t-MCAO) model rat as a cerebral infarction and reperfusion model. Brain cell damage after the reperfusion was assessed by 2, 3, 5-triphenyltetrazolium chloride (TTC) staining. To clarify a time-dependent change of the integrity of BBB, fluorescein isothiocyanate (FITC)-dextran (150 kDa) was injected intravenously into t-MCAO rats, and time-dependent localization of FITC-dextran was monitored in ex vivo. As a result, obvious brain damage was firstly observed at 3 h after reperfusion following 1 h of MCAO. In contrast, the leakage of FITC-dextran from cerebral vessels was observed immediately after the reperfusion. The present data suggest that the integrity of BBB failed prior to the occurrence of serious brain damage induced by ischemia–reperfusion, and that macromolecules such as water-soluble polymers and proteins which cannot pass through the BBB under normal condition would reach brain parenchyma at early stage after reperfusion. These findings would be useful to establish a novel treatment strategy for reperfusion injury after cerebral infarction.

1. Introduction

The BBB strictly limits material exchange in the brain, which makes drug delivery to the brain tissue difficult. However, it is known that the integrity of the BBB fails after cerebral ischemia and reperfusion, resulting in increase in cerebrovascular permeability (Yang and Betz, 1994). Several factors including reactive oxygen species, matrix metalloprotease (MMP)-2, and -9, vascular endothelial growth factor (VEGF) are considered to be related with increase in permeability by change of cerebral vascular tonus and disruption of basement membrane after reperfusion following cerebral stroke (Rosenberg et al., 1998; Zhang et al., 2002).

In the treatment of cerebral stroke, ischemic penumbra is one of the most important concepts (Lo, 2008). It is defined as ischemic but still viable cerebral tissue. This area recovers if cerebral blood flow is rapidly improved. The aim of treatment for acute phase of cerebral stroke is to recover cerebral blood

* *Corresponding author.* Fax: +81 54 264 5705.
E-mail address: oku@u-shizuoka-ken.ac.jp (N. Oku).

0006-8993/$ – see front matter © 2010 Elsevier B.V. All rights reserved.
doi:10.1016/j.brainres.2010.01.039

flow and to revive the function of neuronal cells in the penumbra. However, many deleterious mediators are upregulated and injure brain tissue by reperfusion after ischemia. For example, reactive oxygen species such as hydrogen peroxide, hydroxyl radicals and superoxide are produced by reperfusion following brain ischemia (Kontos, 2001). They cause cerebral vasodilatation, resulting in brain tissue injury. In fact, α-amino-3-hydroxy-5-methylisoxasolepropionic acid (AMPA) is known to mediate superoxide generation, and the inhibition of AMPA receptor improves ischemic outcome (Erdo et al., 2005). Many other pathways are also involved in secondary brain lesion after cerebral infarction (Cunningham et al., 2005; Huang et al., 2006). This cerebral ischemia–reperfusion injury substantially influences prognosis and mortality of patients treated with thrombolytic agents for cerebral infarct therapy. Therefore, improvement of ischemia–reperfusion injury is essential for the treatment of cerebral ischemia and required to protect a cerebral neuronal cell. Although mechanisms of reperfusion injury after cerebral infarction have been widely studied in the world, clinically available drug at present is only Radicut® (edaravone), a free radical scavenger, for cerebral neuroprotection during cerebral ischemia/reperfusion (Yoshida et al., 2006).

In the case of acute disease such as cerebral infarction, therapeutic time window (TTW) is an important concept. It is defined as the promising time to achieve therapeutic efficacy. For example, tissue plasminogen activator (t-PA), a thrombolytic agent, for treatment of cerebral stroke is decided to inject within 3 h because it has prospects of worsening symptoms more than 3 h after ischemia (Marler and Goldstein, 2003).

t-MCAO model rats by a filament method are used to the study of ischemia–reperfusion injury after focal ischemia (Nagasawa and Kogure, 1989). This method can make a stable cerebral occlusion model using a nylon uniformly coated with silicon. In addition, reperfusion is induced easily by pulling the thread out of the artery. Since this model needs no materials such as t-PA to induce reperfusion, the influences of reperfusion can be observed directly without considering superfluous factors.

Macromolecules with biocompatibility and size above 40 kDa possess long-circulating characteristic in bloodstream, and tend to localize at the site where the vascular permeability is increased (Seymour et al., 1995). In fact, vascular permeability is known to increase at inflammatory site, and a dendritic polymer complexed with ibuprofen is reported to localized and retained at the inflammatory site resulting in a high anti-inflammatory effect (Kannan et al., 2004; Svenson, 2009). Moreover, in myocardial ischemia/reperfusion that shows similar pathological event to cerebral ischemia/reperfusion, macromolecular agents accumulated in the infarction zone at early stage by vascular permeability increase (Lukyanov et al., 2004). However it isn't known that time-dependent change in the extent of diffusion of macromolecules into brain tissue by disruption of the BBB after cerebral ischemia/reperfusion in acute phase.

In the present study, we attempted to clarify the time-dependent relationship between ischemia–reperfusion damage and localization of macromolecules by increasing BBB permeability in t-MCAO model rats for the purpose of the determination of effective term for the treatment of reperfusion injury using macromolecular drugs or drugs in macromolecules.

2. Results

2.1. *Brain damage assessment*

The time-dependent change of ischemia/reperfusion damage was assessed by TTC staining. A ratio between right and left hemisphere section areas represents brain edema. When this ratio significantly exceeds 1, edema is induced on the side of the occlusion. Fig. 1 shows representative photographs of the brain damage in the t-MCAO rats. Total brain slice areas and damaged ones are calculated by Image J, and their mean values are shown in Table 1. The damage of the brain tissue was firstly observed in the section of the MCA at 3 h after the reperfusion. At 6 h after the reperfusion, the damage was observed more broadly than at 3 h, and the cell death progressed to cerebral cortex. Moreover, the most widespread damage was observed at 24 h after the reperfusion. Similarly, the brain edema was firstly observed at 3 h after the reperfusion. However, significant cerebral damage was not observed until 3 h after the reperfusion.

2.2. *Leakage of FITC-dextran*

Time course of the change in cerebral blood vessel permeability after reperfusion in the t-MCAO rat were monitored by the leakage of FITC-dextran with in vivo imaging system. Fig. 2 shows the leakage of FITC-dextran into brain parenchyma at 1 h after the administration. Table 2 shows average of total photon counts obtained from five rats at each time. Interestingly, the leakage of the FITC-dextran from cerebral vessels was observed immediately after the reperfusion in the t-MCAO rat model. This leakage was observed up to 6 h but not at 24 h after the reperfusion. The FITC-dextran localization in brain tissue became broadly as time advances within 3 h. However, the fluorescence intensity was diminished at 6 h compared with that at 3 h.

In the present study, we did not use the same slices in both TTC staining and FITC imaging due to the technical limitation. However the slices were obtained essentially by the same procedure except the injection of FITC-dextran in the latter experiment. Therefore, both TTC staining and FITC imaging would be comparable.

3. Discussion

In the present study, the reperfusion was performed by withdrawing the filament at 1 h after the occlusion using t-MCAO model rats. Although nerve cells suspend electrical activity under ischemic condition, their life is maintained for a few hours because of conservation of ion gradient and cellular membrane pump function (Back, 1998). Therefore, the damage observed in the present study could be mainly derived from reperfusion. Taken together, most of the penumbra area might be protected from death by restoration of blood flow if a treatment for neuroprotection is performed within therapeutic time window.

Cells death of the core infarct area arises predominantly from necrosis, whereas cell death of penumbra area is caused

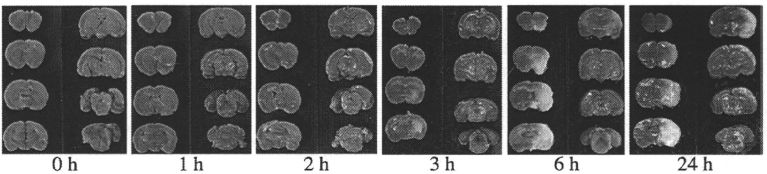

Fig. 1 – Photographs of brain sections prepared from the t-MCAO model rats. The damaged regions were visualized by TTC staining after a 1 h-infarct following 0, 1, 2, 3, 6 or 24 h reperfusion. White areas show the damaged regions and red areas show surviving regions.

mainly by apoptosis following cerebral ischemia (Dirnagl et al., 1999; Lopez-Sanchez et al., 2007; Xu et al., 2006). Therefore, an antiapoptotic agent would protect neuronal cells and attenuate reperfusion injury. In fact, pretreated inhibition of caspase-3 results in decrease of cerebral damage in the penumbra area following 2 h infarct (Zhu et al., 2004). Apoptosis is a key factor improving reperfusion injury, and the detail researches contribute to a new treatment strategy for ischemia–reperfusion injury.

The BBB dysfunction results in cerebral edema, hemorrhage formation and neuronal cell death after cerebral infarction. On the other hand, it permits some drugs that cannot penetrate the BBB in normal condition to reach brain parenchyma. Therefore, it would be one of the promising strategies for improving ischemia–reperfusion injury to delivery agents to brain tissue from cerebral blood flow by increasing BBB permeability. Opening of the BBB has been studied by using many tracers in ischemia/reperfusion. After 2 h occlusion and 3 h reperfusion caused great increase in BBB permeability, which was monitored by the uptake of sucrose (Rosenberg et al., 1998). In the present study, we determined the leakage of macromolecule in more acute phase ischemia/reperfusion. The leakage of FITC-dextran into brain tissue was observed just after the reperfusion in the t-MCAO rat model. These data suggest that tight junction of the BBB fails by reperfusion or 1 h infarct and thus macromolecules such as dextran leak out from bloodstream into the brain tissue. Our findings are consistent with previous reports: For example, a function of myogenic tone, which favors partial vasoconstriction and plays an important role in regulation of cerebrovascular blood flow in response to changes in perfusion pressure, was diminished at early stage after ischemia (Cipolla et al., 1997; Cipolla and Curry, 2002). MMP-2 derived from astrocyte increases at 3 h after reperfusion in the same model rat as the present study (Yang et al., 2007). Therefore, this data suggest that upregulation of MMP-2 is greatly associated with the present result that leakage of FITC-dextran was most broadly at 3 h after reperfusion. Hydroxyl radicals that are one of the most reactivity free radicals greatly increase at immediately after reperfusion in the same model rat as the present study (Kato et al., 2003). Free radicals are related with BBB disruption on how to directly attack cerebral endothelial cells and to mediate MMPs. This report is also associated with the result in the present study. Focusing on the result of 0, 1 and 3 h after reperfusion, fluorescence of FITC-dextran was observed at nearby MCA. In addition, the leakage of FITC-dextran was outspread as time advances. Therefore, BBB disruption progress gradually with time by partial infarct, in this study case is by MCA, after reperfusion.

Table 1 – Time-dependent change of brain injury.

Times after reperfusion	Total volume (cm^3)	Damage volume (cm^3)	Right brain/ left brain
0 h	1.60±0.02	0	1.00±0.00
1 h	1.61±0.02	0	1.01±0.01
2 h	1.61±0.07	0	1.01±0.01
3 h	1.70±0.03	0.05±0.06	1.04±0.02*
6 h	1.72±0.06	0.27±0.07	1.06±0.01**
24 h	1.81±0.05	0.42±0.03	1.12±0.04**

Values are means±SD; $n=5$. Right brain/left brain shows the degree of edema. Statistical differences were calculated by one-way analysis of variance (ANOVA) followed by Dunnett's multiple comparison tests as compared with 0 h after reperfusion group. (*$p<0.05$, **$p<0.01$).

When neuroprotective agents are delivered to brain tissue for the treatment of ischemia–reperfusion injury by enhanced permeability of a failed BBB, a time widow from appearance of BBB disruption to disappearance of it is very important notion. The integrated data demonstrated that the increase of cerebral vascular permeability from BBB dysfunction was occurred at stages before generation of obvious cerebral cell damage in the t-MCAO model rats. This is important information for the treatment and prevention of reperfusion injury. In general, therapeutic agents for acute phase treatment are beneficial as early injection as possible. However, it is also quite important to know until when do these agents are effective after ischemia–reperfusion. For this reason, here we evaluated the permeability change in BBB and brain damage after ischemia–reperfusion to set TTW in acute phase disease. From the present results, we propose that TTW of reperfusion injury is from immediately after reperfusion up to 3 h. At 6 h after the reperfusion, the brain tissue was broadly impaired, and the leakage of FITC-dextran was diminished, hence suggesting that the possibility to save brain cells is lowered. Obvious cerebral cell death was rarely observed up to 3 h after the reperfusion, and the localization of FITC-dextran was observed earlier than outset of the obvious cerebral cell death. Therefore, some treatments before 3 h after reperfusion are

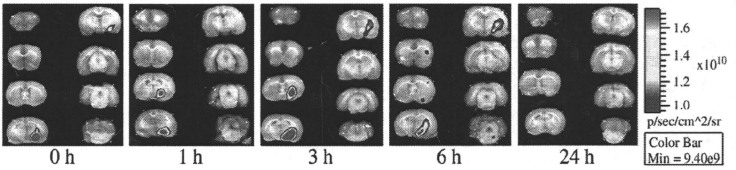

Fig. 2 – The leakage of FITC-dextran in the t-MCAO model rats. Time-dependent change in the integrity of BBB after the reperfusion was monitored by the leakage of FITC-dextran. The t-MCAO rats were injected with FITC-dextran solution (15 mg/ rat i.v.). FITC-dextran localized in the brain sections was visualized with IVIS. Bar shows the relative level of fluorescence intensity, ranging from low (blue), to medium (green), to high (yellow, red). This is the representative from five independent animal experiments, all of which demonstrated similar profile of responses.

expected to be significantly effective for the improvement in reperfusion injury.

In conclusion, macromolecules leaked out from blood-stream into brain parenchyma before the obvious cerebral cell death appeared in t-MCAO model rats, and this localization was broadly more than the damage area at 3 h after the reperfusion. The present study suggests that an approach within 3 h after reperfusion is important and promising for the treatment or prevention of reperfusion injury to provide great therapeutic response.

4. Experimental procedures

4.1. *Animal*

Male Wistar rats (8 weeks old) weighing 170–210 g were purchased from Japan SLC Inc. (Shizuoka, Japan). The animals were cared according to the Animal Facility Guidelines of the University of Shizuoka. All animal experiments were approved the by the Animal and Ethics Review Committee of the University of Shizuoka.

4.2. *Preparation of t-MCAO model rat*

Transient middle cerebral artery occlusion (t-MCAO) was induced by inserting a filament into internal carotid artery (Nagasawa and Kogure, 1989). Anesthesia was induced with 3% isoflurane and maintained with 1.5% one during cerebral stroke surgery. Rectal temperature was maintained at 37 °C with heating pad. After a median incision of the neck skin, the right carotid artery, external carotid artery, and internal carotid artery (ICA) were isolated with careful conservation of the vagal nerve. A 4-0 monofilament nylon suture coated with silicon was introduced into the right ICA and advanced into the origin of the MCA. A silk ligated the MCA at side of inserting point. After the operation, the neck was closed and anesthesia was discontinued. Success of the surgery was judged by the appearance of hemiparesis. Reperfusion was performed by withdrawing the filament about 10 mm at 1 h after the occlusion under isoflurane anesthesia in this all study.

Table 2 – Total photon counts of brain sections.

Injection time	Ischemic side ($\times 10^7$)	Nonischemic side ($\times 10^7$)
0 h	4.18±0.32*	3.58±0.16
1 h	5.71±1.28*	3.64±0.69
3 h	6.70±2.47*	3.83±0.57
6 h	4.21±1.11	3.37±0.59
24 h	4.09±0.67	3.83±0.38

Values are means±SD; $n=5$. Accumulation of FITC-dextran in the brain was determined as described in the legend of Fig. 2. Total photon counts were obtained from the IVIS images. Total photon counts of ischemic side are significantly higher than those of nonischemic side at 0, 1 and 3 h. (*$p<0.05$).

4.3. *Brain damage assessment in t-MCAO rat*

The ischemia/reperfusion damage in the t-MCAO rat model was assessed by morphometric analysis of the brain sections stained with 2, 3, 5-triphenyltetrazolium chloride (TTC, Wako Pure Chemical Ind. Ltd., Tokyo, Japan). The brain was dissected at 0, 1, 2, 3, 6 or 24 h after reperfusion and sliced into 2 mm thick coronal sections using a rat brain slicer (Muromachi Kikai, Tokyo, Japan). These sections were stained with 2% TTC in PBS for 30 min at 37 °C. Then, they were fixed in 10% formalin neutral buffer solution. All sections were put in grass slides and photographed with a digital camera (OLYMPUS E-300). We measured the unstained area, the stained area and each hemisphere with an image analysis system (NIH Image J). The damage regions were considered as completely white area. Edema was calculated from a ratio between right and left hemisphere sections area.

4.4. *Leakage of FITC-dextran into brain tissue*

Time-dependent change of the integrity of BBB after reperfusion was determined using fluorescein isothiocyanate (FITC)-dextran (150 kDa, Sigma-Aldrich, Saint Louis, MO, USA) as a macromolecule. FITC-dextran (0.5 mL) dissolved in saline (30 mg/mL) was injected via a tail vain of the t-MCAO rat model at 0, 1, 3, 6 or 24 h after reperfusion, respectively. One

hour after the injection, the brain was dissected and sliced into 2 mm thick coronal sections in the exactly same way as above experiment. All sections were put in grass slides and their fluorescence was measured at with in vivo imaging system (IVIS, Xenogen Corp., Alameda, CA).

REFERENCES

Back, T., 1998. Pathophysiology of the ischemic penumbra—revision of a concept. Cell. Mol. Neurobiol. 18, 621–638.

Cipolla, M.J., McCall, A.L., Lessov, N., Porter, J.M., 1997. Reperfusion decreases myogenic reactivity and alters middle cerebral artery function after focal cerebral ischemia in rats. Stroke 28, 176–180.

Cipolla, M.J., Curry, A.B., 2002. Middle cerebral artery function after stroke: the threshold duration of reperfusion for myogenic activity. Stroke 33, 2094–2099.

Cunningham, L.A., Wetzel, M., Rosenberg, G.A., 2005. Multiple roles for MMPs and TIMPs in cerebral ischemia. Glia 50, 329–339.

Dirnagl, U., Iadecola, C., Moskowitz, M.A., 1999. Pathobiology of ischaemic stroke: an integrated view. Trends Neurosci. 22, 391–397.

Erdo, F., Berzsenyi, P., Andrasi, F., 2005. The AMPA-antagonist talampanel is neuroprotective in rodent models of focal cerebral ischemia. Brain Res. Bull. 66, 43–49.

Huang, J., Upadhyay, U.M., Tamargo, R.J., 2006. Inflammation in stroke and focal cerebral ischemia. Surg. Neurol. 66, 232–245.

Kannan, S., Kolhe, P., Raykova, V., Glibatec, M., Kannan, R.M., Lieh-Lai, M., Bassett, D., 2004. Dynamics of cellular entry and drug delivery by dendritic polymers into human lung epithelial carcinoma cells. J. Biomater. Sci. Polym. Ed. 15, 311–330.

Kato, N., Yanaka, K., Hyodo, K., Homma, K., Nagase, S., Nose, T., 2003. Stable nitroxide Tempol ameliorates brain injury by inhibiting lipid peroxidation in a rat model of transient focal cerebral ischemia. Brain Res. 979, 188–193.

Kontos, H.A., 2001. Oxygen radicals in cerebral ischemia: the 2001 Willis lecture. Stroke 32, 2712–2716.

Lo, E.H., 2008. A new penumbra: transitioning from injury into repair after stroke. Nat. Med. 14, 497–500.

Lopez-Sanchez, C., Martin-Romero, F.J., Sun, F., Luis, L., Samhan-Arias, A.K., Garcia-Martinez, V., Gutierrez-Merino, C., 2007. Blood micromolar concentrations of kaempferol afford protection against ischemia/reperfusion-induced damage in rat brain. Brain Res. 1182, 123–137.

Lukyanov, A.N., Hartner, W.C., Torchilin, V.P., 2004. Increased accumulation of PEG-PE micelles in the area of experimental myocardial infarction in rabbits. J. Control. Release 94, 187–193.

Marler, J.R., Goldstein, L.B., 2003. Medicine. Stroke—tPA and the clinic. Science 301, 1677.

Nagasawa, H., Kogure, K., 1989. Correlation between cerebral blood flow and histologic changes in a new rat model of middle cerebral artery occlusion. Stroke 20, 1037–1043.

Rosenberg, G.A., Estrada, E.Y., Dencoff, J.E., 1998. Matrix metalloproteinases and TIMPs are associated with blood–brain barrier opening after reperfusion in rat brain. Stroke 29, 2189–2195.

Seymour, L.W., Miyamoto, Y., Maeda, H., Brereton, M., Strohalm, J., Ulbrich, K., Duncan, R., 1995. Influence of molecular weight on passive tumour accumulation of a soluble macromolecular drug carrier. Eur. J. Cancer. 31A, 766–770.

Svenson, S., 2009. Dendrimers as versatile platform in drug delivery applications. Eur. J. Pharm. Biopharm. 71, 445–462.

Xu, X.H., Zhang, S.M., Yan, W.M., Li, X.R., Zhang, H.Y., Zheng, X.X., 2006. Development of cerebral infarction, apoptotic cell death and expression of X-chromosome-linked inhibitor of apoptosis protein following focal cerebral ischemia in rats. Life Sci. 78, 704–712.

Yang, G.Y., Betz, A.L., 1994. Reperfusion-induced injury to the blood-brain barrier after middle cerebral artery occlusion in rats. Stroke 25, 1658–1664 discussion 1664-5.

Yang, Y., Estrada, E.Y., Thompson, J.F., Liu, W., Rosenberg, G.A., 2007. Matrix metalloproteinase-mediated disruption of tight junction proteins in cerebral vessels is reversed by synthetic matrix metalloproteinase inhibitor in focal ischemia in rat. J. Cereb. Blood Flow Metab. 27, 697–709.

Yoshida, H., Yanai, H., Namiki, Y., Fukatsu-Sasaki, K., Furutani, N., Tada, N., 2006. Neuroprotective effects of edaravone: a novel free radical scavenger in cerebrovascular injury. CNS Drug Rev. 12, 9–20.

Zhang, Z.G., Zhang, L., Tsang, W., Soltanian-Zadeh, H., Morris, D., Zhang, R., Goussev, A., Powers, C., Yeich, T., Chopp, M., 2002. Correlation of VEGF and angiopoietin expression with disruption of blood–brain barrier and angiogenesis after focal cerebral ischemia. J. Cereb. Blood Flow Metab. 22, 379–392.

Zhu, H.C., Gao, X.Q., Xing, Y., Sun, S.G., Li, H.G., Wang, Y.F., 2004. Inhibition of caspase-3 activation and apoptosis is involved in 3-nitropropionic acid-induced ischemic tolerance to transient focal cerebral ischemia in rats. J. Mol. Neurosci. 24, 299–305.

Journal of Controlled Release 141 (2010) 208–215

Contents lists available at ScienceDirect

Journal of Controlled Release

journal homepage: www.elsevier.com/locate/jconrel

Temperature-dependent transfer of amphotericin B from liposomal membrane of AmBisome to fungal cell membrane

Kosuke Shimizu [a], Masaaki Osada [a], Koji Takemoto [b], Yutaka Yamamoto [b], Tomohiro Asai [a], Naoto Oku [a,*]

[a] Department of Medical Biochemistry and Global COE program, School of Pharmaceutical Sciences, University of Shizuoka, 52-1 Yada, Suruga-ku, Shizuoka 422-8526, Japan
[b] Dainippon Sumitomo Pharma Co., Ltd., 1-98 Kasugade Naka 3-Chome, Konohana-ku, Osaka 554-0022, Japan

ARTICLE INFO

Article history:
Received 18 April 2009
Accepted 22 September 2009
Available online 6 October 2009

Keywords:
AmBisome
Temperature-dependency
Cell wall
Ergosterol
Membrane fluidity

ABSTRACT

Liposomal amphotericin B (AMPH-B), also known as AmBisome, exhibits a potent antifungal effect through its binding to ergosterol contained within the fungal cell membrane. However, the mechanism responsible for the movement of AmBisome-derived AMPH-B to the fungal cell membrane through the cell wall is not yet clear. Therefore, in the present study we aimed at elucidating this mechanism operating in *Saccharomyces cerevisiae*. AmBisome showed its antifungal effect against *S. cerevisiae* at 35 °C but not at 4 °C, whereas free AMPH-B was effective at both temperatures. A significant difference in the amount of AMPH-B transferred to the fungal cells between incubation at 4 and 35 °C was also observed when AmBisome was used. Confocal microscopic study, however, indicated that NBD-labeled AmBisome was localized on the surface of the fungal cells at either temperature. To decrease the affinity of AMPH-B for the liposomal membrane, we entrapped AMPH-B in fluid liposomes containing egg yolk phosphatidylcholine (EPC) instead of hydrogenated soy PC (HSPC). These liposomes showed the antifungal effect even at 4 °C. On the contrary, AMPH-B in liposomes containing ergosterol (Erg-AmB) instead of cholesterol showed a significantly weaker antifungal effect at 35 °C with reduced transfer of AMPH-B to the fungal cells. These results suggest that not the binding of AmBisome to target cells but the transfer of AMPH-B from liposomal membrane of AmBisome to the cell membrane is critical for the antifungal activity of AmBisome. This transfer is dependent on the temperature, fluidity of the liposomal membrane, and the affinity of AMPH-B for the fungal cell membrane.

1. Introduction

Since patients with infectious diseases caused by certain bacteria or fungi are at a high risk for death, the development of effective drugs for these diseases is of great importance. Mycosis is an infectious disease caused by fungal invasion, and it is divided into 3 classes based on the infection site. Among them, infection by fungi at deep internal organ such as lung and brain is the most serious and is known as deep mycosis. Amphotericin B (AMPH-B), a drug with strong antifungal activity, is effective against deep mycosis and also has a wide antibacterial spectrum [1,2]. As to its mechanism of action, AMPH-B is known to bind to ergosterol contained in the fungal cell membrane, which binding induces a permeability change in the membrane [3,4]. Since AMPH-B also has the ability to bind to cholesterol to some extent [5], it causes side effects such as nephrotoxicity [6]. In order to reduce the side effects of AMPH-B, a liposomal formulation of AMPH-B, known as AmBisome, has been developed. AmBisome is a small unilamellar vesicle containing AMPH-B that is stably retained in the hydrophobic part of the liposomal membrane by complexing with liposomal cholesterol. Since liposomalization of AMPH-B prolongs the circulation of AMPH-B in the bloodstream and decreases the transfer of AMPH-B to cell-membrane cholesterol, the use of AmBisome reduces the side effects of AMPH-B [7–11]. The mechanism of transfer of AMPH-B from AmBisome to the fungal membrane is still unclear, since AmBisome retains the drug in the liposomal membrane rather tightly. By electron microscopy Adler-Moore et al. previously examined the localization of liposomal lipids of AmBisome after exposure to fungal cells such as *Candida glabrata* and *Aspergillus fumigatus* and observed that AmBisome-derived lipids were distributed throughout the cytoplasm of the fungal cells after long-term incubation [12,13]. They also speculated that AmBisome has an affinity for the fungal cell wall and initially binds to it and that the liposomal lipids from AmBisome become dispersed throughout the cytoplasm after damage to the fungal cell membrane caused by AMPH-B released from disrupted AmBisome [13]. Their report indicates that the transfer of AmBisome-derived AMPH-B to the fungal cell membrane is a key step in the action of AmBisome against fungi.

In the present study, we aimed at elucidating the mechanism underlying the transfer of AMPH-B from AmBisome to the fungal cell membrane by using *Saccharomyces cerevisiae* as a model fungal cell. *S. cerevisiae* has a thick cell wall similar to that of other fungal cells [14].

Abbreviations: AMPH-B, amphotericin B; EPC, egg yolk phosphatidylcholine; EPG, egg yolk phosphatidylglycerol; DSPG, distearoylphosphatidylglycerol; HSPC, hydrogenated soy phosphatidylcholine; NBD-PE, *N*-4-nitrobenzo-2-oxa-13-diazol phosphatidylethanolamine.

* Corresponding author. Tel.: +81 54 264 5701; fax: +81 54 264 5705.
E-mail address: oku@u-shizuoka-ken.ac.jp (N. Oku).

0168-3659/$ – see front matter © 2009 Elsevier B.V. All rights reserved.
doi:10.1016/j.jconrel.2009.09.019

At first, we examined the temperature dependence of AmBisome activity against *S. cerevisiae*, and observed that, unlike AMPH-B, the antifungal activity of AmBisome was drastically suppressed at a low temperature. Then, we examined the localization of AmBisome in yeast cells at different temperatures by confocal laser-scanning microscopy and measured the amount of AMPH-B taken up into the cells. The transfer of AMPH-B from AmBisome to the cell and the antifungal activity of the liposomes were increased by raising the incubation temperature. Interestingly, AMPH-B in a fluid liposomal membrane was taken up into the cells more easily and was fungicidal at a low temperature. On the contrary, AMPH-B in ergosterol-containing liposomes was taken up into the cells in less amount; and the cytotoxic action was suppressed even at a high temperature. The results indicate the importance of translocation of AMPH-B from AmBisome to the cells in its antifungal activity.

2. Materials and methods

2.1. Reagents

AmBisome was the product of Dainippon Sumitomo Pharma Co., Ltd. (Osaka, Japan) Hydrogenated soy phosphatidylcholine (HSPC), distearoylphosphatidylglycerol (DSPG), egg yolk phosphatidylcholine (EPC), egg yolk phosphatidylglycerol (EPG), and cholesterol were gifts from Nippon Fine Chemical Co., Ltd. (Hyogo, Japan). Amphotericin B (AMPH-B), ergosterol, and *N*-4-nitrobenzo-2-oxa-13-diazol phosphatidylethanolamine (NBD-PE) were purchased from The United States Pharmacopeial Convention, Inc. (Rockville, MD, U.S.A.), Sigma-Aldrich Co. (St Louis, MO, U.S.A.), and Avanti Polar Lipids, Inc. (Alabaster, AL, U.S.A.), respectively. Rhodamine-dextran (10 kDa) was purchased from Wako Pure Chemical Industries, Ltd.

2.2. Yeast cell culture

Yeast cells of the *S. cerevisiae* ATCC 9763 (ATCC, U.S.A.) were used as a model of fungal cells in this experiment. They were colonized on YPD/agar medium and kept at 4 °C. Before experimental use, a single colony was picked up and grown in YPD medium with shaking at 30 °C for at least 12 h; and the OD_{600} of the cell suspension was adjusted to 0.1 using RPMI 1640 medium (Sigma-Aldrich Co.) buffered to pH 7.0 with 0.165 M MOPS (Dojindo Laboratories, Kumamoto, Japan).

2.3. Preparation of liposomes

AmBisome (liposomal AMPH-B) was composed of HSPC, DSPG, cholesterol, and AMPH-B (10:4:5:2 as a molar ratio). AmBisome solution was prepared by hydration of lyophilized AmBisomal components with ultrapure water. For preparation of NBD-labeled AmBisome, the lyophilized AmBisomal components were firstly dissolved in chloroform, after which NBD-PE solution was added to them. Then, they were lyophilized again with *t*-butanol and rehydrated with succinate-buffered solution (pH 5.5). Unincorporated NBD-PE was removed by gel filtration chromatography with a PD-10 column. For preparation of AmBisome encapsulating rhodamine-dextran, the lyophilized AmBisomal components were hydrated with rhodamine-dextran solution; and then free rhodamine-dextran was removed by column chromatography with Sepharose™ 4 Fast Flow (GE Healthcare UK Ltd., England). AMPH-B in liposomes containing ergosterol (Erg-AmB) was prepared with HSPC, DSPG, ergosterol, and AMPH-B (10:4:5:2 as a molar ratio). The thin lipid film containing AMPH-B was hydrated with succinate-buffered solution with 9% sucrose at 60 °C and freeze-thawed with liquid nitrogen for 3 cycles. The obtained liposomal solution was sized by sonication. Unincorporated AMPH-B was removed by column chromatography with Sepharose™ 4 Fast Flow. Liposomal AMPH-B composed of highly fluid phospholipids (Egg-AmB) was prepared with EPC, EPG, cholesterol, and AMPH-B (10:4:5:2 as a molar ratio) in the similar manner as used to prepare Erg-AmB. The particle size of each liposome was measured by dynamic light scattering analysis with a Zetasizer Nano (Malvern Instruments, Malvern, U.K.) and was about 100 nm in diameter.

2.4. Colony formation assay

Each liposomal AMPH-B diluted in succinate-buffered solution with 9% sucrose or free AMPH-B dissolved in 0.1% DMSO (final conc.) at a concentration of 20 μM as AMPH-B was added to a yeast cell suspension and incubated in MOPS-buffered RPMI 1640 medium at 4 or 35 °C for 0.5 or 3 h. Then, the cell suspension was centrifuged and washed twice with PBS. The cell pellet was resuspended in PBS and plated on YPD/agar medium. After 24 h of incubation at 30 °C, the number of colonies formed was counted.

2.5. Confocal microscopy

NBD-labeled liposomal AMPH-B (20 μM) was added to a yeast cell suspension, which was then incubated in MOPS-buffered RPMI 1640 medium at 4 or 35 °C for 3 or 24 h with shaking. After having been washed 3 times with PBS, the cells were fixed with 4% paraformaldehyde and stained with Fluorescent Brightener 28 (Sigma-Aldrich Co., U.S.A.) for cell-wall imaging. After another 3 washes with PBS, the cells were attached to MAS-coated glass slides (Matsunami Glass Ind., Ltd., Japan) by centrifugation, and then localization of liposomes in yeast cells was observed under an LSM510 META confocal laser-scanning microscope (Carl Zeiss, Inc., Germany).

2.6. Measurement of the amount of AMPH-B transferred to yeast cells

Liposomal AMPH-B (20 μM) was added to a yeast cell suspension, which was then incubated in MOPS-buffered RPMI 1640 medium with shaking at 4 or 35 °C for 0.5 or 3 h. After having been washed with PBS, the cells were disrupted by using glass beads with shaking and sonication, and AMPH-B in the cells was extracted with methanol. After centrifugation, the methanol extract was evaporated; and the residual AMPH-B was dissolved in the mobile phase for HPLC analysis. The HPLC conditions were the following: Column, TSKgel ODS-100Z 4.6×250 mm (Tosoh Co., Japan); mobile phase, acetonitrile and 2.5 mM EDTA (pH 5.0), 4:6 (v/v); temperature, 35 °C; injection volume, 50 μL; flow rate, 1.0 mL/min; and UV detection, 405 nm. Smart Chrom software was used for control of the HPLC system and data processing.

In the inhibition experiment, AmBisome was added to a yeast cell suspension, which was subsequently incubated in the presence or absence of drug free cholesterol liposomes (Cho-Lip) or vacant ergosterol liposomes (Erg-Lip) in MOPS-buffered RPMI 1640 medium. After a 3-h incubation, the amount of AMPH-B transferred to the cells was measured.

2.7. Investigation of AmBisome disruption

Rhodamine-encapsulating AmBisome was added to different numbers of yeast cells (OD_{600} = 0.1 or 0.3), and the cells were incubated in MOPS-buffered RPMI 1640 medium for 0.5 or 3 h at 4 or 35 °C. After centrifugation for washing, the supernatant medium was collected and ultracentrifuged to separate the intact AmBisome into the pellet. The resulting supernatant was then collected, and the fluorescence intensity of the rhodamine-dextran that had been released into the medium from AmBisome was measured.

2.8. FRAP experiment

NBD-labeled AmBisome and Egg-AmB were similarly prepared as described above and then gradually frozen to make giant-sized liposomes. Then, these liposomes were applied on MAS-coated slide glasses and dried in the dark at room temperature for overnight. FRAP experiments were performed with LSM510 META confocal laser-